LBL-19035
UC-95

Lawrence Berkeley Laboratory
UNIVERSITY OF CALIFORNIA

APPLIED SCIENCE DIVISION

RECEIVED
LAWRENCE
BERKELEY LABORATORY

APR 8 1985

LIBRARY AND
DOCUMENTS SECTION

ELECTRODELESS HID LAMP STUDY:
Final Report

J.M. Anderson, P.D. Johnson, C.E. Jones,
and T.H. Rautenberg

January 1985

TWO-WEEK LOAN COPY
This is a Library Circulating Copy
which may be borrowed for two weeks.

APPLIED SCIENCE
DIVISION

Prepared for the U.S. Department of Energy under Contract DE-AC03-76SF00098

LBL-19035 c.2

DISCLAIMER

This document was prepared as an account of work sponsored by the United States Government. While this document is believed to contain correct information, neither the United States Government nor any agency thereof, nor the Regents of the University of California, nor any of their employees, makes any warranty, express or implied, or assumes any legal responsibility for the accuracy, completeness, or usefulness of any information, apparatus, product, or process disclosed, or represents that its use would not infringe privately owned rights. Reference herein to any specific commercial product, process, or service by its trade name, trademark, manufacturer, or otherwise, does not necessarily constitute or imply its endorsement, recommendation, or favoring by the United States Government or any agency thereof, or the Regents of the University of California. The views and opinions of authors expressed herein do not necessarily state or reflect those of the United States Government or any agency thereof or the Regents of the University of California.

LBL-19035
EEB-L 85-01
L-97

ELECTRODELESS HID LAMP STUDY: FINAL REPORT

J.M. Anderson,* P.D. Johnson,* C.E. Jones,* and T.H. Rautenberg*

Lighting Systems Research Group
Lawrence Berkeley Laboratory
University of California
Berkeley CA 94720

January 1985

This work was supported by the Assistant Secretary for Conservation and Renewable Energy, Office of Building Energy Research and Development, Buildings Equipment Division of the U.S. Department of Energy under Contract No. DE-AC03-76SF00098.

* General Electric Company
Corporate Research and Development
Schenectady NY 12301

Subcontract No. 4522010

ABSTRACT

High intensity discharge lamps excited by solenoidal electric fields (SEF/HID) were examined for their ability to give high brightness, high efficacy and good color. Frequency of operation was 13.56 MHz (ISM Band) and power to the lamp plasma ranged from about 400 to 1000 W. Radio frequency transformers with air cores and with air core complemented by ferrite material in the magnetic path were used to provide the voltage for excitation. Electrical properties of the matching network and the lamp plasma were measured or calculated and total light from the lamp was measured by an integrating sphere. Efficacies calculated from measurement were found to agree well with the positive column efficacies of conventional HID lamps containing only mercury, and with additives of sodium, thallium, and scandium iodide. Recommendations for future work are given.

ACKNOWLEDGEMENTS

Design of the experiments and their setup, calibration, and conduct was by J.M. Anderson and C.E. Jones. Mr. Jones was especially responsible for digital acquisition of data and for computer programming. P.D. Johnson specified ingredients for the arc envelopes and filled them. He also interpreted the data in relation to known HID technology. T.H. Rautenberg acquired and processed spectral data. V.D. Roberts provided managerial assistance. The contractual support from The Department of Energy is gratefully acknowledged.

This work was supported by the Assistant Secretary for Conservation and Renewable Energy, Office of Building Energy Research and Development, Buildings Equipment Division of the U.S. Department of Energy under Contract No. DE-AC03-76SF00098.

TABLE OF CONTENTS

Section		Page
1	INTRODUCTION	1
2	LAMP EXCITATION	5
3	ARC TUBE PROCESSING	9
4	EXPERIMENTAL PROCEDURE AND SAMPLE CALCULATION	11
5	RESULTS	21
6	DISCUSSION	37
7	CONCLUSIONS AND RECOMMENDATIONS FOR FUTURE WORK	41
8	REFERENCES	43
A	APPENDIX A-DETERMINATION OF THE COUPLING COEFFICIENT BY BRIDGE MEASUREMENTS	45
B	APPENDIX B-SOME COMMENTS ON PRIMARY COIL DESIGN	47
C	APPENDIX C-DESIGN AND CALIBRATION OF THE POWER MEASUREMENT EQUIPMENT	53
D	APPENDIX D-SKIN DEPTH CONSIDERATIONS	57
E	APPENDIX E-IMPEDANCE MATCHING CONSIDERATIONS	61

LIST OF ILLUSTRATIONS

Figure		Page
1	Sketch of the lamp and ferrite core assembly used in early tests	5
2	Sketch of the lamp and ferrite assembly shown in Figure 1, giving dimensions and placement of the excitation coil	6
3	Cross section of the electrodeless lamp assembly using only an excitation coil without ferrite cores.	7
4	Expected shape of the resistance and reactance reflected from the ring of lamp arc plasma into the primary circuit	11
5	Equivalent circuit of the lamp and matching network used to calculate electrical quantities	16
6	Calibration curves to determine coil and circuit loss based upon measured current I_5 of Figure 5	17
7a	View of the electrodeless lamp in the one-meter integrating sphere, along with the standard metal-halide lamp	23
7b	Close-up of the electrodeless lamp	24
8	Spectra of lamp SL3 at 486 W into the arc plasma	30
9	Spectra of lamp SL3 at 821 W into the arc plasma	30
10	Spectra of lamp SL3 at 1040 W into the arc plasma	31
11	Spectra of lamp SL4 at 1092 W into the arc plasma	31
12	Spectra of lamp SL5 at 493 W into the arc plasma	32
13	Spectra of lamp SL5 at 1151 W into the arc plasma	32
14	Spectra of lamp SL7 at 390 W into the arc plasma	33
15	Spectra of lamp SL7 at 698 W into the arc plasma	33
16	Measured efficacies of lamp SL3, 4, 5, 7, and 8 as a function of power delivered to the arc plasma	34
17	Calculated voltage gradient along the arc column (circumference of the arc ring) for various tested SEF/HID lamps	34
18	Calculated arc current for various SEF/HID lamps tested	35
19	RF resistance of a solenoidal coil of wire (lowest curve) as the wire diameter is varied	49
20	Input resistance to a solenoidal coil of wire (No. 8 gauge) as the height of the coil is varied	50
21	Sketch of the voltage and current pickoff assembly	54

LIST OF ILLUSTRATIONS (Cont'd)

Figure		Page
22	Simplified sketches of the matching network between the coaxial transmission line and the primary coil which couples to the lamp plasma secondary	62
23	Schematic of the relation between the primary coil and the power source	63

LIST OF TABLES

Table		Page
1	Printout of Impedance Matching to the Arc Plasma	13
2	Printout of Input Impedance to a Wire Solenoid as Frequency Is Varied	15
3	Lamp Sizes and Ingredients	22
4	Calculations for Lamp SL3	25
5	Calculations for Lamp SL4	26
6	Calculations for Lamp SL5	27
7	Calculations for Lamp SL7	28
8	Calculations for Lamp SL8	29
9	Wavelength Distribution of Optical Energy	39

Section 1

INTRODUCTION

The work reported herein was performed under contract No. 4522010 with Lawrence Berkeley Laboratories, Berkeley, California and its purpose was to demonstrate the operation of high intensity discharge (HID) lamps excited with solenoidal electric fields (SEF). The SEF/HID lamp has no electrodes, the arc current being continuous and closing upon itself within the arc containing envelope. The electric field is created by a changing magnetic field, and is thus solenoidal or divergence free. Specifically, the goals of this program were to:

1. Assemble a light-producing module operating with power input at 13.56 MHz and consisting of the arc plasma and envelope, the solenoidal drive coil with a magnetic path which may contain ferrite material, and the matching network which adjusted the lamp impedance to the coaxial line from the power source.
2. Construct and fill at least three arc envelopes with ingredients commonly used in metal halide HID lamps.
3. Instrument an integrating sphere so that the SEF/HID lamp and a standard HID lamp could be placed therein. Design and construct a power measuring set-up to accurately measure power at a frequency of 13.56 MHz to the lamp. Arrange to measure the photometric output from the sphere and to measure the spectrum of light emitted from the lamp.
4. Verify and calibrate the system stated under 3.
5. Make measurements with an RF impedance bridge on the lamp assembly as necessary to allow calculation of the pertinent voltages and currents in the circuit and lamp.
6. Make electrical and optical measurements on at least three lamps to determine the behavior of the lamps, especially their efficacy. The starting date of this contract was October 15, 1983.

Electrical gaseous discharge lamps have developed over the past 50-year period into high efficiency light sources. For example, the high pressure sodium lamp produces over 120 lumens of light per watt of electrical power, and its application to roadway lighting is now extensive. However, all commercially available discharge lamps use electrodes to convey the discharge maintenance current to and from of the lamp envelope. These electrodes are responsible for a number of design and performance limitations in current HID lamps. Electrodes waste substantial amounts of energy, especially in the smaller size lamps. For example, in typical 400-watt HID lamps, the electrodes consume 10% of the lamp power while producing very little light.[1] In lower wattage lamps suitable for residential applications, the loss can be as high as 30%, since the approximately constant electrode drop is a bigger fraction of the smaller lamp voltage.

In addition, HID lamp life is limited by electrode degradation phenomena such as loss of activator material, dissolution of tungsten in a molten silicon condensate, and other processes associated with the intrinsically high temperature of any electrode. These electrode related problems are more evident in lamps that are started frequently. Electrodes often suffer from a design compromise because they are required to operate as anodes half of the time and cathodes the other half.[2]

The most interesting electrode related design compromise may be that fill materials in standard electroded lamps must be chemically compatible with the electrodes themselves, thus eliminating many advantageous materials from consideration as lamp radiating media. For example, the chlorides and bromides of aluminum, tin and mercury promise significant improvements in discharge lamp color and efficacy. Aluminum chloride has been shown to produce continuum radiation in the visible region of the spectrum[3], possibly due to molecular transitions in the chlorine molecule, although free-bound transitions have not yet been ruled out. Unfortunately, use of these chlorides in standard arc tubes results in chemical attack of the electrodes. Therefore, the mechanism of light output and possible advantages of these materials or other chlorides have not been fully explored.

There is a need to develop an electrodeless lamp design which would avoid all of these electrode related difficulties. Most importantly, an electrodeless lamp offers the possibility of new, improved lamp fills which could not be considered in a lamp with electrodes. In this work a program was conducted which led to operation of HID lamps without electrodes. Lamps with conventional fills of mercury and the iodides of sodium, thallium and scandium were operated and recommendations made for unconventional lamp fills which may have better efficacy and color.

Electrodeless discharges in gases have a long history. In 1891, J.J. Thompson, Cavendish Laboratory, Cambridge, described a "ring" discharge in gases created by radio frequency magnetic fields. His transformer had an air core, and such air core excitation of gases has shown advantage in many research applications, including the current nuclear fusion program.

An early electrodeless high pressure mercury lamp using an iron-core transformer was suggested by Morrison in 1929.[4,5]

A survey of visual observations on electrodeless discharges created by electric fields, as well as by magnetic induction, was made by George Babat.[6] He referred to them respectively as E and H discharges. Recently a more complete survey was assembled by Eckert.[7] His emphasis was on atmospheric pressure induction discharges which might be used industrially for crystal growing or optical fiber manufacture.

Various workers have examined high pressure inductive discharges for the purpose of light generation, but none have been developed into commercial applications, except a class of low pressure lamps used for spectroscopic purposes. Hollister patented a spherical quartz envelope driven with power sources operating at frequencies of about 30 MHz or higher.[8,9] Yamamoto uses an iron core to excite high intensity discharges in a toroidal lamp envelope.[10] Operating at much higher frequencies, about 1000 MHz, small spherical arc tubes have been excited by a combination of E and H discharges at GTE Laboratories.[11–14]

Falling electronics costs and the availability of better semiconductor switching devices offer the promise of cost effective high frequency electronic ballasting for an electrodeless lamp in the near future.

Simultaneously, the General Electric Research and Development Center has pursued an electrodeless HID lamp based on high-pressure mercury-metal halide technology. Patents were granted for electrodeless lamps using ferrite cores in 1967 and 1970.[15,18] Recently a configuration especially adapted to HID discharges was patented.[19] Optimum operation for the range of lamp powers and physical sizes studied was found to occur at the upper end of the frequency range, 0.5 to 3 MHz, when the coupling characteristics and loss in the ferrite material were considered.

Some operational and design problems of electrodeless HID lamps were identified in these early programs. One technical limitation was heat loss from the discharge to the inner wall of the quartz toroid. The discharge tended to rest close to this inner wall rather than in the center of the envelope. At the high power loading, which is known to give high efficacy, excessive heating of the wall resulted.

In the current work, reported here, the discharge envelope was redesigned to be in the general shape of a pill box, having no inner wall. The primary excitation coil must necessarily be located somewhat removed from the lamp plasma and the magnetic coupling path must be partly of air. Nevertheless lamp excitation can be effected and results are reported herein.

Section 2

LAMP EXCITATION

In this work lamps were excited by solenoidal electric fields (SEF) using a solenoidal coil that had either an air core or air core complemented by ferrite material. The lamp requires a voltage gradient in the gaseous plasma in order to impart energy to the free electrons of the plasma, and this gradient is produced by a changing magnetic field in the transformer core. For example, the plasma discharge ring in the lamp might require 200 V (rms) around the circumference of a circle of diameter 3.8 cm. This implies a field of 0.00207 Tesla or 20.7 Gauss (rms) at 13.56 MHz excitation frequency. If this field is obtained, also as an example, from a one-turn loop having a diameter of 6.9 cm, the current in the loop must be 114 A. Of course, there can be several turns in the loop to reduce the current per turn, but voltage across the loop (coil) terminals increases accordingly, and this presents its special problems as discussed in Appendix B. There is considerable incentive to incorporate ferrite material in part or all of the magnetic path for its value in reducing the current necessary in the coil. The improvement is describable in terms of an increase in the coupling coefficient as discussed in Appendix A.

The initial design for a primary coil/ferrite core assembly used in this work is sketched in Figure 1. Toroidal cores of Q-1 material, manufactured by Indiana General Company,

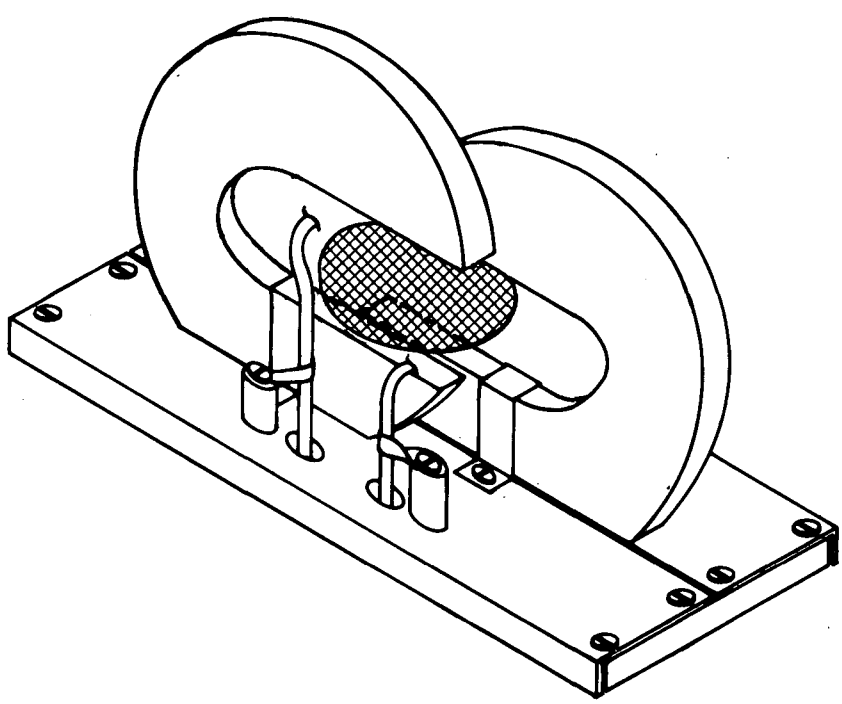

Figure 1. Sketch of the lamp and ferrite core assembly used in early tests. The cores are toroidal, cut to accommodate the lamp envelope. The excitation coil is not shown to reduce confusion.

were cut as shown to accommodate the discharge envelope and coil. The primary coil is not shown in this figure to reduce confusion. Figure 2 shows the cross section of envelope, coil, and cores. The coupling coefficient with this arrangement was measured to be 0.48 and the input reactance at 13.56 MHz without the lamp operating was 416 Ω. Experiments with this assembly and difficulties encountered will be described in the next section.

For the bulk of this work an air core transformer was used to excite the HID lamps, see Figure 3. It consisted of a primary coil having eight turns with mean diameter 2.5 in. (6.35 cm) and height 1.8 in. (4.57 cm). The wire was 0.125-in. (0.317 cm) copper tubing, silver-plated to a thickness of about one mil (0.025 mm). The coil was supported with its central axis vertical above an aluminum box 5×3×7 in. which contained the matching network. Teflon tubing carried cooling water in and out of the coil ends.

The discharge was contained in a pill-box shaped quartz envelope about 5.5 cm in diameter and 2 cm high. In turn, the envelope was located in a quartz outer container which had a lid for quick change to other arc envelopes. The general arrangement is shown on Figure 3.

The bridge-measured coupling coefficient for the coil/plasma geometry of Figure 3 was 0.316 (see Appendix A). This was considerably less than that with partial ferrite cores and the price paid was additional loss in the coil due to the higher currents needed. However, for the intended purpose of exciting the SEF/HID lamps, it worked well and permitted a good measurement of positive column efficacy.

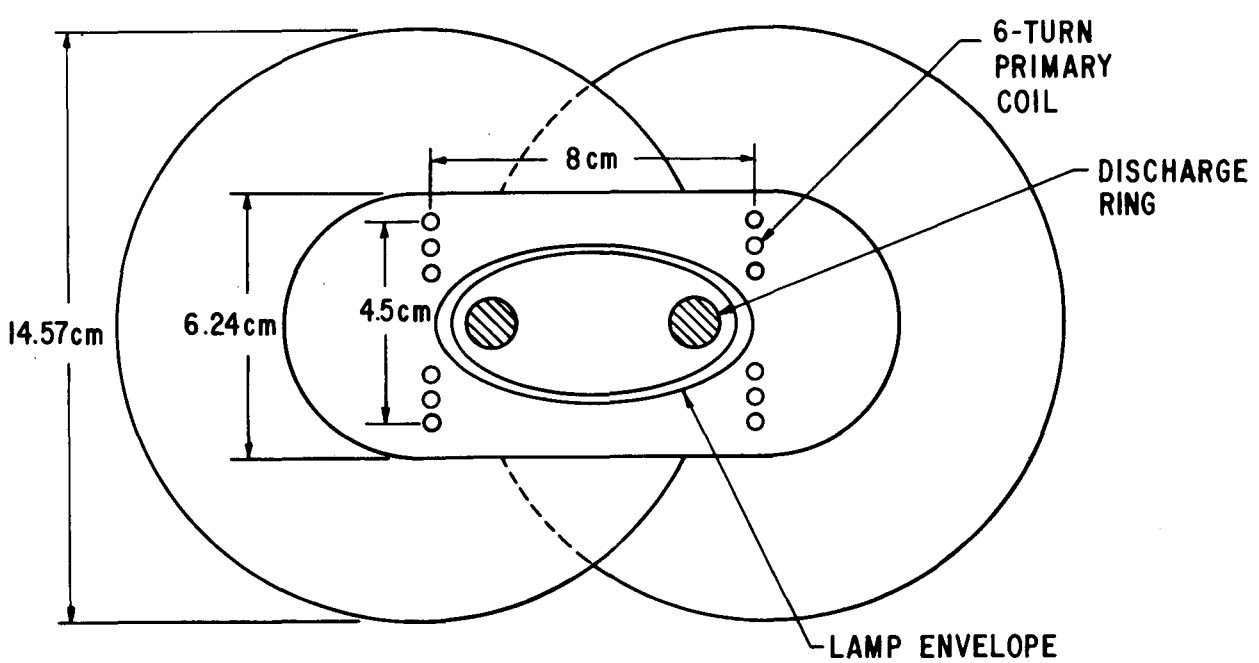

Figure 2. Sketch of the lamp and ferrite assembly shown on Figure 1, giving dimensions and placement of the excitation coil.

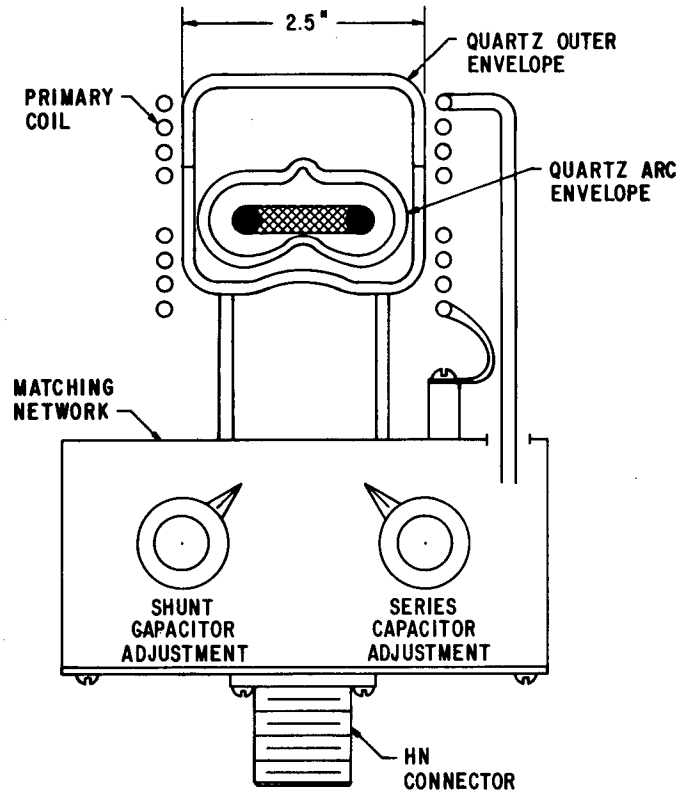

Figure 3. **Cross section of the electrodeless lamp assembly using only an excitation coil without ferrite cores. The coil is eight turns of one-eighth-inch copper tubing, silver-plated. The lower aluminum box contains both series and shunt matching capacitors. The quartz arc envelope is enclosed in an openable quartz container for quick change of arc envelopes.**

Section 3

ARC TUBE PROCESSING

An important difference between processing the electrodeless and conventional electroded discharge tubes is in the requirement for outgassing before dosing. Because of the extensive work with the hydrogen flames required to form the electrodeless tubes, the fused quartz becomes heavily loaded with water. We have found it necessary to vacuum bake the arc tubes at 1050 °C for about 12 hours. One arc tube that was not vacuum baked because of scheduling priorities was extremely difficult to start. Although vacuum baking has been found desirable in the commercial production of metal halide arc tubes, it is a necessity for the electrodeless tubes used in the present work. The requirement for vacuum baking could undoubtedly be eliminated by using plasma torches to fabricate the tubes.

Conventional arc tubes are usually backfilled with an inert gas on the exhaust equipment and an arc is operated briefly both to activate the electrodes and for further removal of contaminants. We replaced this step with a back fill of about 50 torr Ar and then established a discharge using a Tesla coil. The discharge was operated while the argon was pumped out. The final fill was 6 to 22 torr Ar, the lower pressure giving easier glow to arc transition in the finished arc tube.

Dosing was done using laboratory scale procedures designed to ensure purity of ingredients and, in particular, freedom from water contamination. All ingredients were attached to the exhaust system near to the arc tube in separate side tubes and were purified by distillation while on exhaust before being driven into the arc tube.

The arc tubes shown in Figure 3 were 5.1 to 5.4 cm o.d., 1.6 to 1.8 cm average outside vertical dimensions and about 1.5 to 2 mm wall thickness giving an internal volume of about 25 cm^3. They were constructed with a convex upward bottom so that the molten halides of the reservoir-temperature-limited doses would be forced to occupy areas of the discharge tube which were heated by the discharge.

Section 4

EXPERIMENTAL PROCEDURE AND SAMPLE CALCULATION

The power source used to excite the lamp was a Henry Radio Model 5KPGB transmitter, crystal-controlled at 13.56 MHz. Under well matched conditions it supplies 5 kW into 50 Ω via a RG218/U coaxial line. In our experiment the line was not well matched during starting and warmup of the lamp, implying considerable power returned to the power source. Power delivery by the source is limited under mismatched conditions, but was still adequate to start lamps. Under operating conditions the match, even if not perfect, was good enough to deliver 2-3 kW or more if needed.

The lamp envelope contains a conducting plasma ring which has both reactance and resistance. Through the drive coil, this impedance is coupled into the primary circuit according to

$$Z_{in} = R_p + j\,X_p + (k^2 X_p X_s)\ x \left[\frac{R_s}{R_s^2 + X_s^2} - j\,\frac{X_s}{R_s^2 + X_s^2} \right] \tag{1}$$

where R_p and X_p are the self resistance and self reactance of the drive coil, k is the coupling coefficient, and R_s and X_s are the resistance and reactance of the secondary (plasma). Thus, the input impedance contains both a resistive and reactive component. Figure 4 shows the variations of reflected resistance and reactance, calculated from equation 1, as the resistance of the secondary plasma ring varies. The reflected resistance is the third term on the right hand side of (1) and the reflected reactance is the fourth term. Note that the reflected resistance peaks, and this occurs about where the secondary resistance and reactance are equal.

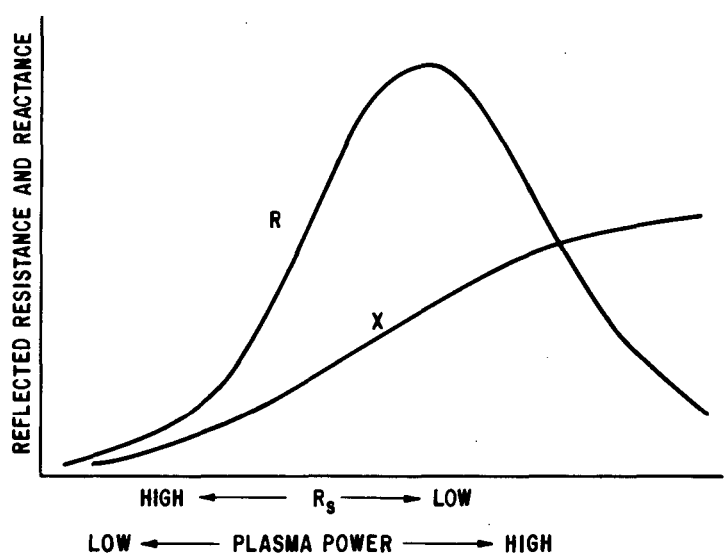

Figure 4. Expected shape of the resistance and reactance reflected from the ring of lamp arc plasma into the primary circuit. The resistance of the arc plasma is varied, which is equivalent to varying power supplied to the discharge.

A simple capacitive impedance matching network was chosen to match the primary coil to the line (50 Ω) from the power source. Under constant conditions of the secondary (lamp plasma), a perfect match could easily be gotten with this well known scheme. In Appendix E we describe how this match is effected. For our case with HID lamp plasmas, the resistance of the secondary can change from a low value upon start to a high resistance in the thermally-stabilized run condition. A short computer program was written to assess the impedance at the drive coil as the secondary resistance changes. With the measured quantities mentioned in Appendix A, namely $X_p = 416\ \Omega$ and $k = 0.48$, the program gave results shown in Table 1. The variables are the discharge field in V/cm and the reactance of the series matching capacitor. Within each block of data, the capacitive reactance is varied, and from block to block, the discharge electric field. The field is low upon lamp starting and increases as the lamp warms. One notes that the impedance seen by the line, last four columns, changes from about 24 Ω at 84 degrees for a "cold" lamp to 51 Ω at zero degrees as the lamp "warms up." The lamp secondary resistance varies from about 1 to 25 Ω. These discharge quantities are only assumed at this point, but are sufficiently realistic to indicate trends. Another interesting point is that the resistance component reflected from secondary to primary, column 6, peaks at about 47 Ω. This agrees with theory for the case where secondary (plasma) resistance and reactance are equal. It was observed experimentally that the input impedance did vary widely during warm up, according to tests on an operating lamp; but the lamp could be started and run by a minimum of adjustment if power levels were kept low during warm up, and increased when the impedance stabilized.

The matching capacitors were the variable vacuum type CMV1 obtained from ITT Jennings, San Jose, California. They could withstand a peak working voltage of 3 kV and carry 40 A continuously. The range of variable capacity was 8 to 1000 pF. The shunt capacitor in the matching network was connected to a short length (33 in., 81.2 cm) of RG 9/U cable which provided a path from the power sensor assembly into the integrating sphere. This length of cable must be regarded in the calculation and is simply treated by transmission line equations that relate input impedance to the terminating impedance, and vice versa. The elements of this are also treated in Appendix E.

Figure 5 shows the equivalent circuit diagram used to calculate the electrical quantities throughout the matching network and the lamp. To the far left of the figure, the power source delivers power through about 3 m of RG18/U cable. The voltage and current sensors supply the digital oscilloscope with line voltage and current, V_1 and I_1. The oscilloscope digitizes their waveforms and calculates the power input and phase angle between V_1 and I_1. This establishes the conditions at point A. A length of RG 9/U cable carries the power to point B. The input impedance calculated at point A is transformed to point B (see Appendix E) by

$$Z_r = Z_o \left[\frac{Z_s \cos \beta l - j\ Z_o \sin \beta l}{Z_o \cos \beta l - j\ Z_s \sin \beta l} \right] \tag{2}$$

where,

Z_r = Terminating impedance at point B,

Z_s = Measured input impedance at point A,

Table 1

PRINTOUT OF IMPEDANCE MATCHING TO THE ARC PLASMA

HIDSEF/MATCH2 03-JAN-84 11:01:53

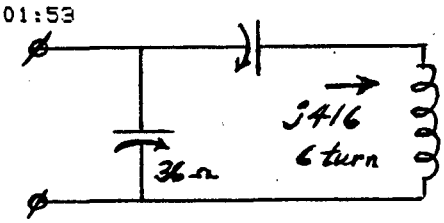

COUPLING COEFFICIENT	0.480
COUP. COEFF. SQUARED	0.230
SECONDARY DIA. (IN)	1.970
CROSS SECT. (IN)	0.394
L SECONDARY (uh)	0.053
X SECONDARY (OHMS)	4.523
SECONDARY POWER (KW)	1.000
PRIMARY # OF TURNS	6.000
Xp	36.000

Xs	Cs	V/CM	Rs	Is	INPUT Z	Ip	Ein	Z TO 50 OHM LINE	
386	30.4	2.0	0.99	31.81	19.99+j325	7.07	2300	2.62-j 23	23@ -84
387	30.3	2.0	0.99	31.81	19.99+j325	7.07	2300	2.57-j 23	24@ -84
388	30.3	2.0	0.99	31.81	19.99+j325	7.07	2300	2.52-j 23	24@ -84
389	30.2	2.0	0.99	31.81	19.99+j325	7.07	2300	2.47-j 24	24@ -84
390	30.1	2.0	0.99	31.81	19.99+j325	7.07	2300	2.42-j 24	24@ -84
391	30.0	2.0	0.99	31.81	19.99+j325	7.07	2300	2.38-j 24	24@ -84
392	29.9	2.0	0.99	31.81	19.99+j325	7.07	2300	2.33-j 24	24@ -84
393	29.9	2.0	0.99	31.81	19.99+j325	7.07	2300	2.29-j 24	24@ -85
386	30.4	3.0	2.22	21.20	37.95+j339	5.13	1750	5.88-j 23	24@ -76
387	30.3	3.0	2.22	21.20	37.95+j339	5.13	1750	5.77-j 23	24@ -76
388	30.3	3.0	2.22	21.20	37.95+j339	5.13	1750	5.66-j 23	24@ -76
389	30.2	3.0	2.22	21.20	37.95+j339	5.13	1750	5.55-j 23	24@ -77
390	30.1	3.0	2.22	21.20	37.95+j339	5.13	1750	5.44-j 24	24@ -77
391	30.0	3.0	2.22	21.20	37.95+j339	5.13	1750	5.34-j 24	24@ -77
392	29.9	3.0	2.22	21.20	37.95+j339	5.13	1750	5.24-j 24	24@ -78
393	29.9	3.0	2.22	21.20	37.95+j339	5.13	1750	5.14-j 24	24@ -78
386	30.4	4.0	3.95	15.90	47.49+j362	4.59	1674	10.44-j 23	25@ -65
387	30.3	4.0	3.95	15.90	47.49+j362	4.59	1674	10.23-j 23	25@ -66
388	30.3	4.0	3.95	15.90	47.49+j362	4.59	1674	10.02-j 23	25@ -66
389	30.2	4.0	3.95	15.90	47.49+j362	4.59	1674	9.82-j 23	25@ -67
390	30.1	4.0	3.95	15.90	47.49+j362	4.59	1674	9.63-j 23	25@ -67
391	30.0	4.0	3.95	15.90	47.49+j362	4.59	1674	9.43-j 23	25@ -68
392	29.9	4.0	3.95	15.90	47.49+j362	4.59	1674	9.25-j 23	25@ -68
393	29.9	4.0	3.95	15.90	47.49+j362	4.59	1674	9.07-j 23	25@ -69
386	30.4	5.0	6.18	12.72	45.68+j383	4.68	1803	16.25-j 22	27@ -54
387	30.3	5.0	6.18	12.72	45.68+j383	4.68	1803	15.90-j 22	27@ -54
388	30.3	5.0	6.18	12.72	45.68+j383	4.68	1803	15.56-j 22	27@ -55
389	30.2	5.0	6.18	12.72	45.68+j383	4.68	1803	15.22-j 22	27@ -55
390	30.1	5.0	6.18	12.72	45.68+j383	4.68	1803	14.90-j 22	26@ -56
391	30.0	5.0	6.18	12.72	45.68+j383	4.68	1803	14.57-j 22	26@ -56
392	29.9	5.0	6.18	12.72	45.68+j383	4.68	1803	14.26-j 22	26@ -57
393	29.9	5.0	6.18	12.72	45.68+j383	4.68	1803	13.95-j 22	26@ -57
386	30.4	6.0	8.90	10.60	38.72+j396	5.08	2024	23.24-j 21	31@ -42
387	30.3	6.0	8.90	10.60	38.72+j396	5.08	2024	22.69-j 20	30@ -42
388	30.3	6.0	8.90	10.60	38.72+j396	5.08	2024	22.15-j 20	30@ -42
389	30.2	6.0	8.90	10.60	38.72+j396	5.08	2024	21.61-j 20	29@ -43
390	30.1	6.0	8.90	10.60	38.72+j396	5.08	2024	21.08-j 20	29@ -43
391	30.0	6.0	8.90	10.60	38.72+j396	5.08	2024	20.56-j 20	28@ -44
392	29.9	6.0	8.90	10.60	38.72+j396	5.08	2024	20.05-j 20	28@ -44
393	29.9	6.0	8.90	10.60	38.72+j396	5.08	2024	19.54-j 20	28@ -45

Table 1 (Cont'd)

Reactance of Series Matching Capacitor	Value of Series Capacitor – pF	Discharge Volts/cm	Discharge Resistance (Secondary)	Discharge Current (RMS) Amps (1 kW)	Input Impedance to Primary	Primary Current Amps (RMS)	Primary Voltage (RMS)	Input Z seen by Power Cable (Rect. Coordinates)	Input Z seen by Power Cable (Polar Coordinates)
386	30.4	7.0	12.11	9.09	31.42+j404	5.64	2288	31.28-j 18	36@ -30
387	30.3	7.0	12.11	9.09	31.42+j404	5.64	2288	30.43-j 18	35@ -30
388	30.3	7.0	12.11	9.09	31.42+j404	5.64	2288	29.58-j 17	34@ -30
389	30.2	7.0	12.11	9.09	31.42+j404	5.64	2288	28.73-j 17	33@ -31
390	30.1	7.0	12.11	9.09	31.42+j404	5.64	2288	27.90-j 17	33@ -31
391	30.0	7.0	12.11	9.09	31.42+j404	5.64	2288	27.07-j 16	32@ -31
392	29.9	7.0	12.11	9.09	31.42+j404	5.64	2288	26.26-j 16	31@ -32
393	29.9	7.0	12.11	9.09	31.42+j404	5.64	2288	25.46-j 16	30@ -32
386	30.4	8.0	15.82	7.95	25.34+j409	6.28	2573	40.17-j 15	43@ -20
387	30.3	8.0	15.82	7.95	25.34+j409	6.28	2573	38.86-j 14	41@ -20
388	30.3	8.0	15.82	7.95	25.34+j409	6.28	2573	37.55-j 13	40@ -20
389	30.2	8.0	15.82	7.95	25.34+j409	6.28	2573	36.25-j 13	38@ -19
390	30.1	8.0	15.82	7.95	25.34+j409	6.28	2573	34.95-j 12	37@ -19
391	30.0	8.0	15.82	7.95	25.34+j409	6.28	2573	33.68-j 12	36@ -19
392	29.9	8.0	15.82	7.95	25.34+j409	6.28	2573	32.43-j 11	34@ -19
393	29.9	8.0	15.82	7.95	25.34+j409	6.28	2573	31.22-j 11	33@ -20
386	30.4	9.0	20.02	7.07	20.61+j411	6.97	2869	49.62-j 10	51@ -12
387	30.3	9.0	20.02	7.07	20.61+j411	6.97	2869	47.65-j 9	48@ -11
388	30.3	9.0	20.02	7.07	20.61+j411	6.97	2869	45.67-j 8	46@ -10
389	30.2	9.0	20.02	7.07	20.61+j411	6.97	2869	43.70-j 7	44@ -9
390	30.1	9.0	20.02	7.07	20.61+j411	6.97	2869	41.77-j 6	42@ -9
391	30.0	9.0	20.02	7.07	20.61+j411	6.97	2869	39.87-j 6	40@ -8
392	29.9	9.0	20.02	7.07	20.61+j411	6.97	2869	38.04-j 5	38@ -8
393	29.9	9.0	20.02	7.07	20.61+j411	6.97	2869	36.27-j 5	37@ -8
386	30.4	10.0	24.71	6.36	16.97+j413	7.68	3172	59.28-j 4	59@ -4
387	30.3	10.0	24.71	6.36	16.97+j413	7.68	3172	56.37-j 2	56@ -2
388	30.3	10.0	24.71	6.36	16.97+j413	7.68	3172	53.46-j 1	53@ -1
389	30.2	10.0	24.71	6.36	16.97+j413	7.68	3172	50.61+j 0	51@ 0
390	30.1	10.0	24.71	6.36	16.97+j413	7.68	3172	47.83+j 1	48@ 1
391	30.0	10.0	24.71	6.36	16.97+j413	7.68	3172	45.16+j 2	45@ 2
392	29.9	10.0	24.71	6.36	16.97+j413	7.68	3172	42.60+j 2	43@ 3
393	29.9	10.0	24.71	6.36	16.97+j413	7.68	3172	40.18+j 2	40@ 3

Table 2

PRINTOUT OF INPUT IMPEDANCE TO A WIRE SOLENOID AS FREQUENCY IS VARIED

```
        ***     COIL INPUT Z          ***

COIL OPERATING TEMPERATURE = 25 Deg C

GEOM. ASSUMPTIONS :
        WIRE TYPE                COPPER
        WIRE SIZE (A.W.G.)       8
        WIRE DIA. (cm)           0.3175
        Rdc (ohms/foot)          6.28E-4

PRIMARY MEAN DIA.   (inches) 2.6
        HEIGHT      (inches) 1.8
        # OF TURNS           8
        C-C SPACING     (cm) 0.5715
             Lp    (uh) = 3.59482642789
             Rdc(ohms) = 0.00382792832319
        Self Cap.,(pF) = 7.67570559172
  Self Res. Freq.,MHz  = 30.2985618237
```

F,MHz	R ac	R in	X in	Q
0.10	0.025	0.025	+2.2870E+000	91.0
0.20	0.035	0.035	+4.5741E+000	129.4
0.50	0.056	0.056	+1.1438E+001	205.7
1.00	0.078	0.078	+2.2894E+001	292.5
2.00	0.110	0.111	+4.5936E+001	414.9
5.00	0.172	0.182	+1.1751E+002	644.8
7.00	0.203	0.226	+1.6900E+002	747.0
10.00	0.241	0.303	+2.5631E+002	845.2
13.56	0.279	0.436	+3.8682E+002	887.8
15.00	0.291	0.511	+4.5304E+002	886.3
17.00	0.308	0.657	+5.6520E+002	860.8
20.00	0.332	1.044	+8.0622E+002	772.2
25.00	0.370	3.628	+1.7762E+003	489.6
30.00	0.403			

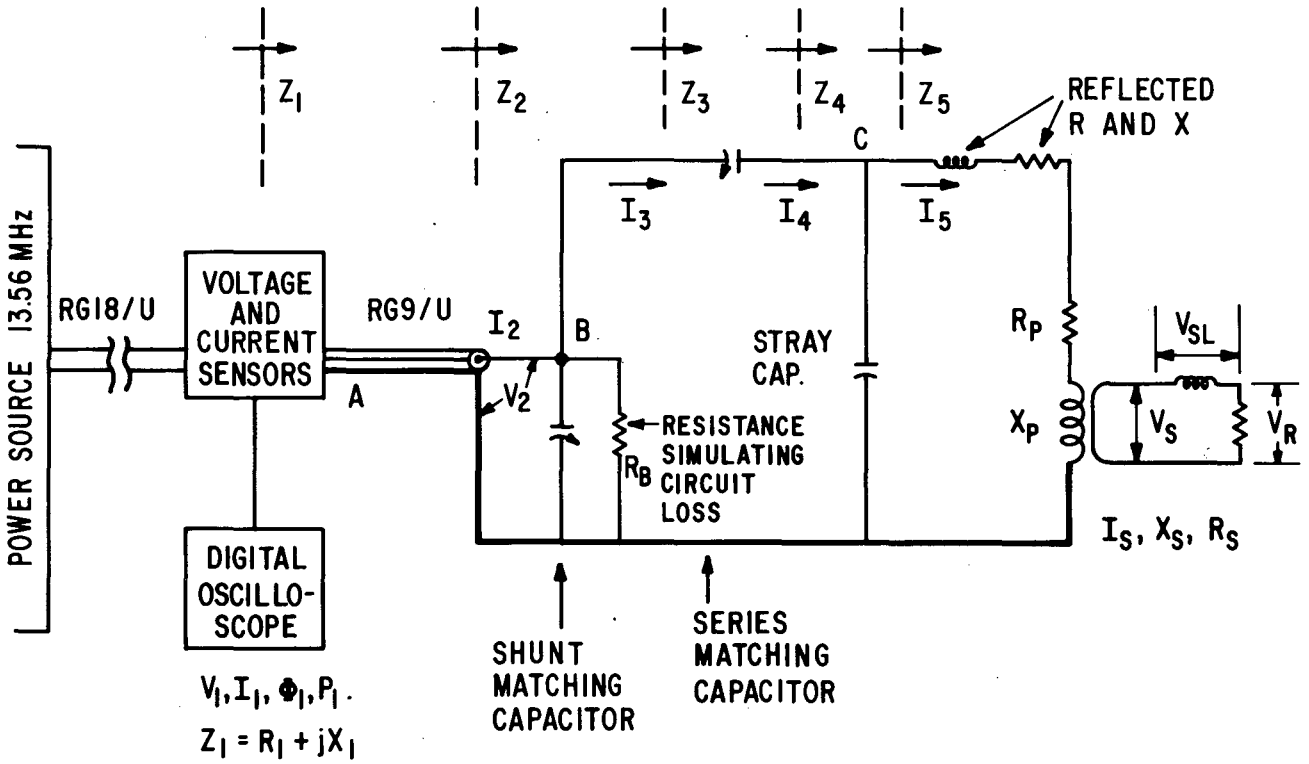

Figure 5. Equivalent circuit of the lamp and matching network used to calculate electrical quantitities. The lamp is represented by resistance R_s and reactance X_s.

Z_o = Characteristic impedance of the cable, 50 Ω,

$\beta = 2\pi/\lambda$, λ is the wavelength in the cable, and

l = length of the cable.

At point B there are three current paths for I_2 to flow into. All have a common voltage, V_2, and so vector algebra with V_2 set to zero degrees, an example of which will be given shortly, quickly tells us I_3. The resistance R_B is chosen to represent, in lumped form, the distributed circuit loss throughout the circuit from point A to point C. The loss might typically be ~40 W and R_B might be one or a few kilo-ohms. Exactly where this loss takes place would be quite difficult to say. Dielectric losses are probably small because no heating of the various insulators is noted. The bulk of the loss is most probably ohmic heating of the various conductors. A small loss for instance takes place in the transmission line (83.82 cm of RG9/U cable), which connects the voltage and current sensors with the matching network within the integrating sphere. This cable has about 0.0055 db/ft or 0.01804 db/m loss at 13.56 MHz. For our cable length and the condition of carrying 1000 W to a matched load, a loss of 3.5 W is anticipated. The wiring of the matching capacitors and the return leads is done with copper braid (3/8 in. wide) to reduce inductance and loss. Still this could give some loss at 13.56 MHz, because the currents through the capacitors can be ~15 A or more. To evaluate the lumped loss, simulated by R_B, the coil loss and total input power are measured as shown on Figure 6 for various values of measured current in the coil. The difference between the readings is taken to be circuit loss. The actual calibration of coil loss is effected by establishing

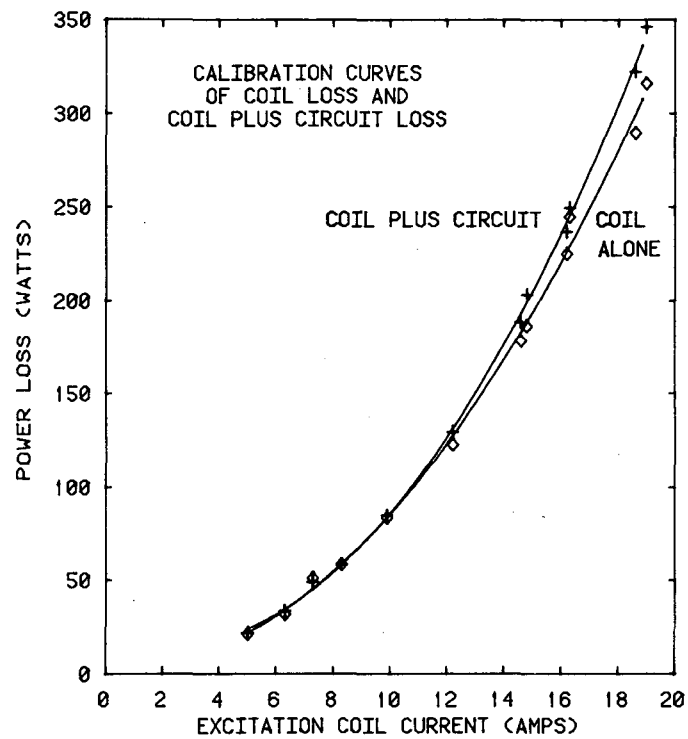

Figure 6. Calibration curves to determine coil and circuit loss based upon measured current I_5 of Figure 5. Data (as crosses and diamonds) are averaged to plot the solid curves.

known currents in the coil and measuring the change in cooling water temperature as the latter passes through the coil. The scheme works quite well, and yields the calibration of Figure 6 as noted above. This procedure establishes currents and losses in the coil and circuit that are similiar, but not exactly equal, to those under actual lamp operation. The differences are small and hard to calculate, but they involve only a few watts, and are thus neglected in comparison to the large power transferred to the discharge plasma.

From point B to point C the reactance of the series matching capacitor, typically $\sim 500\ \Omega$ for the air core excited lamp, alters only the reactive component of the impedance (X_3 goes to X_4). Stray capacity has a very strong influence upon the impedance Z_4 as seen at point C. It tends to enhance both the resistive and reactive components of impedance Z_5 as discussed in Appendix C. The reflected R and X as indicated on Figure 5 can next be referred through the previously measured coupling coefficient to the lamp discharge ring finally determining X_s and R_s.

During an experiment the following quantities are measured:

- Input current at A.
- Input voltage at A.
- Current I_2 (as a check)
- Shunt matching capacitance.
- Current I_5 (as a check)
- Light level in the integrating sphere.
- Differential coil cooling water temperature.

These measurables permit a fairly complete calculation, as will be carried out in the following for the case of a lamp filled with 3 atmospheres of mercury vapor when operating at a plasma input power of 769.6 W. For reference the case chosen is that for the third row of data in Table 5.

Measured was:

$I_1 = 2.85$ A

$V_1 = 323.0$ V (I lags V by 9.5 degrees)

$I_2 = 3.60$ A

$I_5 = 16.75$ A

Sphere output = 37,848 lm

Shunt capacitance = 360 pF

Parallel resonance of primary and lead wire = 24.5 MHz

$Z_1 = Z_s$ calculates to 111.77 + j 18.78 Ω and $P_1 = 907.82$ W. After referral through the transmission line, $Z_R = Z_2 = 65.71 + j\,46.94\ \Omega$. A fuller statement of this is given in Appendix E. The power level at this point is 907.82 W, therefore I_2 is found by the resistive component of Z_2 to be 3.72 A. A current meter at this point measured 3.60 A. I_2 into the impedance Z_2 gives $V_2 = 300.16$ V. Since V_2 is common to several shunt circuits it is convenient to set it to zero angle in a vector diagram. From Figure 6 and I_5 (measured) the circuit loss is found to be 18.29 W and the primary coil loss to be 241.84 W. Voltage V_2 and 18.29 W into R_B determines R_B at 4926.7 Ω. Z_3 becomes 6.45 + j 24.73 Ω after the necessary vector algebra.

Now the first parallel resonance of the primary coil and its associated circuitry, including the stray capacity of the input terminal of the series matching capacity, was determined with a grid dip meter to be 24.5 MHz. To do this the series matching capacitor must be disconnected from the coil. The resistive component of Z_3, namely 6.45 Ω, now transforms (see Appendix B, Equation B-4) according to

$$6.45\left[1-\left(\frac{13.56}{24.5}\right)^2\right]^2 = 3.10 = R_5\,.$$

It is clear that R_5 is composed of the reflected resistance from the plasma and R_p. We can pro-rate these resistances on the basis of power loss because we know that 241.84 W is lost in the coil and 647.7 W goes on to the discharge plasma. This gives us:

$$\text{Reflected resistance} = 2.259 = \frac{647.7}{889.5}\ X\ (3.10)$$

and

$$R_p \qquad = .8433 = \frac{241.84}{889.5}\ X\ (3.10)$$

I_5 into 3.10 Ω (with a total power of 889.5 W transferred to R_5) can be calculated at 16.94 A. It was measured at 16.75 A, which is a reasonably good agreement.

Use of Equation (1) will permit calculation of R_s and X_s but first we must know the coupling coefficient, k, and L_s, the inductance of the plasma ring. The latter is observed to have a major diameter of about 3.9 cm and minor diameter of about 0.5 cm as far as the ring of greatest brightness is concerned. This gives an inductance (see reference 20, page 143) of 0.0584 μH and a reactance, X_s, of 4.98 Ω. The coefficient k was determined separately, see Appendix A, to be 0.316 and $k^2 = 0.1$. The calculated inductance of the primary coil (from Equation B-1 in Appendix B) gives $X_p = 306.3$ Ω at 13.56 MHz. From all this, R_s and X_s are determined as

$$R_s = 67.12$$

$$X_s = 4.98$$

A power of 647.7 W is delivered to the secondary and thus the secondary current is 3.11 A using the above resistive component. This current through R_s and X_s gives voltage drops of 208.5 and 15.46 V, respectively. Only the "resistive" voltage, 208.5 V, is responsible for plasma excitation. The total secondary voltage is the vector sum of these two voltages and becomes 209.07 V. At this point we can note that the secondary voltage gradient is 17.06 V/cm and the power loading is 52.86 W/cm of column length. These numbers agree generally well with what one would expect for the positive column of an electroded arc in 3 atmospheres of mercury at DC or low frequencies. It should be noted that a strict comparison between electroded and electrodeless arcs cannot be made because of the dissimilar geometries. This will be discussed later.

Return for a moment to the difference between Z_3 and Z_4, which difference should be the reactance of the series matching capacitor. The net reactance, X_5, is composed of the primary coil reactance 306.3 reduced by the reflected reactance, which in this case calculates to 0.167 Ω. The latter is neglected compared to 306.3 Ω in this and later calculations. However, the reactive component of Z_5 is modified by the resonating effect of the stray capacity according to (Appendix B, Equation B-3)

$$X_4 = X_5 \left[1 - \left(\frac{13.56}{24.5}\right)^2\right]^{-1} = 441.8\ \Omega$$

Now the series tuning reactance converts this to $X_3 = 24.73$ Ω (inductive), so 441.8 - 24.73 = 417.07 Ω (capacitive) for this capacitor. Its value is thus 28.1 pF.

There is one other interesting calculation which can be made, even if it is approximate because the assumptions are not strictly correct. We have calculated the primary current, I_5, equal to 16.94 A, and the primary reactance equal to 306.3 Ω. Their product gives a voltage across the primary = 5189 V. But there are eight turns, and so volts/turn = 648.6. The coupling coefficient is 0.316 and (0.316) X (648.6) = 204.9 V, which is essentially the 209 V we calculate. The assumption of assigning the mutual flux only to that fraction from the primary is incorrect. However, one can note that the squared ratio of diameters of the plasma ring (3.9 cm) and the mean diameter of the primary (6.9 cm) equals 0.319, quite close to the coupling coefficient we measure, namely 0.316. We are in effect comparing areas for the case of uniform magnetic flux density, again not strictly correct but helpful for "rule of thumb."

Finally, we determined from the output of the calibrated integrating sphere that the total light was 37,848 lm and this divided by power to the discharge, 647.69 W, gives a "positive column" efficacy of 58.45 lm/W.

This detailed example has been carried out for the case of air-core excitation. It would have followed somewhat the same lines if the core was fully or partly of ferrite material, the major difference being that loss in the ferrite material would have to be measured and an equivalent resistance added to R_p; or an equivalent shunt resistance may be assigned across L_p, whichever seems the most appropriate.

Section 5

RESULTS

Initial tests were made outside the integrating sphere using a lamp assembly which had partial ferrite cores. Sketches of the lamp assembly are shown in Figure 1 and Figure 2, and measurement of the coupling coefficient is described in Appendix A. The quartz lamp envelopes were in the shape of a flattened spheroid with dimensions about 4.5 cm by 8 cm. The ingredients with which these lamps were filled are listed on Table 3. Lamps SL1 and SL2 were the size just described while the rest of the lamps on Table 3 were smaller and used in the fully air-core setup.

When SL1 and SL2 were first started the discharge was quite diffuse, appearing to fill the entire envelope. As mercury pressure increased, the arc took the shape of a toroidal ring. It shrank in both major and minor diameter as the mercury pressure approached atmospheric or greater until finally it was about 5 cm in major diameter and 0.6 cm in minor diameter. The arc resembled closely the arc one sees in a conventional electroded lamp. This is to be expected because the skin depth, see Appendix D, for electromagnetic penetration is larger than the arc dimensions and RF heating of the plasma electrons is little different than dc heating. The arc was only lightly wall-stabilized but still stable and steady in light output. There were none of the obvious instabilites one sometimes sees in metal halide lamps at lower frequencies of excitation, ~20 kHz. We were above acoustic resonances of any discernible magnitude.

Both lamps were brought to equilibrium temperature (all mercury vaporized) and electrical measurements were made. After some effort, calculations and measurements were brought into reasonable agreement for power inputs to SL1 of 730 W and 995 W and to SL2 for 1150 W. These will not be discussed here in any detail because, as described in the next paragraph, ferrite core excitation was abandoned in the following work.

A very considerable radiation heating of the ferrite core pole pieces resulted in cracking the ferrite material due to non-uniform expansion. This could have been corrected by appropriate shields and perhaps water or conduction cooling. Also the ferrite surfaces could have been painted white for measurements in the integrating sphere. However, it was questionable whether this would have been worth the effort, especially because the power levels for stable operation in the ferrite core configuration were approximately 1000 W, and the interest expressed by LBL was for lower power levels. Thus, the decision was made to move to a fully air-core configuration as shown on Figure 3.

A photograph of the SEF/HID lamp assembly as it is mounted in the light integrating sphere is shown in Figure 7. Both the SEF/HID lamp and the standard metal halide lamp were in the sphere at all times to maintain the same light absorption. Lamps SL3 through SL8, exclusive of SL6 which could not be started, were operated over a power range of about 400 to 1000 W into the plasma. All lamps easily started in the electric mode, that is they discharged due to the electric field of the coil with displacement current passing through the quartz envelope. Higher voltage was necessary in all cases to get into the solenoidal mode where plasma current is entirely divergence-free within the envelope. Lamp SL8 was filled with a lower rare gas pressure, see Table 3, and although it appeared somewhat easier to start, it still remained a problem. We had the capability to go to 25 A in the primary coil without flashover, and this implied ~300 V around the discharge path. All lamps started in the SEF mode when freshly made but after the first run-up in power they became much more difficult to get into the desired mode. The possibility remains

Table 3

LAMP SIZES AND INGREDIENTS

Lamp SL#	SAE	Fill Hg (Atmos.)	NaI mg	TlI mg	ScI_3 mg	Argon Pressure (Torr)
1	4.5X8cm	1	-	-	-	20.0
2	"	2.5	-	4	-	21.5
3	2X5.5cm	2	42	5.4	-	20
4	"	3	-	-	-	20
5	"	2	-	1.7	-	19
6	"	2	69	-	10.0	20
7	"	2.5	42.6	2.6	6.4	21.5
8	"	2.5	49.0	4.6	-	7.0

Note, #6 could not be started

that there was some outgassing of the quartz envelope or ingredients when hot, or that after the first operation some traces of iodine were present. This was especially true if the lamps were shut off while operating at very high power levels, above 1000 W. In the practical design of a SEF/HID lamp, this question of starting will require attention.

Printouts of the calculated data for the lamps operated are shown on Tables 4 through 8. These data are representative and are plotted on Figures 16, 17 and 18. The latter figures contain some additional plotted data not noted on the tables. The first five columns show measured data and are V_1, I_1, ϕ_1, I_5, and the photodetector output indicating light level in the integrating sphere. All additional columns are calculated according to the procedure of the previous section. The column headed R_s is the discharge plasma resistance per cm of arc path.

For selected lamps, and for various power levels, the spectrum was observed. These are shown in Figures 8 through 15 for lamps and powers as tabulated:

SL3	486.3, 821.1, and 1040.3 W
SL4	1092.5 W
SL5	493.1, and 1151.7 W
SL7	390.2, and 698.3 W

A composite of efficacies for the lamps tested is shown in Figure 16, the variation of column voltage gradient in Figure 17 and arc current in Figure 18. Discussion of these results will be made in the next section of this report.

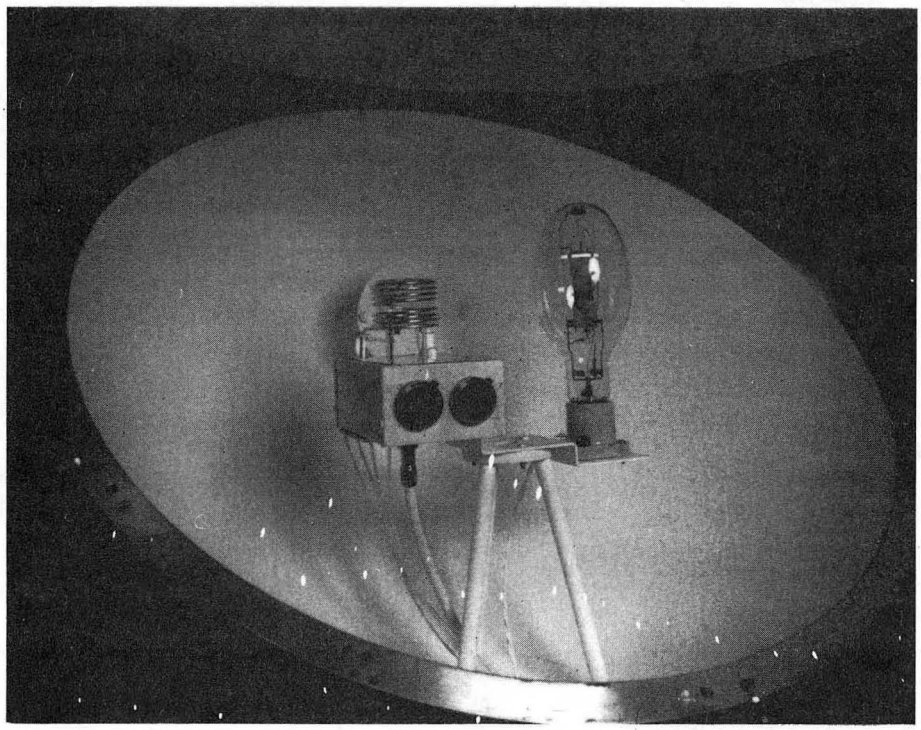

Figure 7a. View of the electrodeless lamp in the one-meter integrating sphere, along with the standard metal-halide lamp. Both lamps remain in the sphere during calibration and measurement.

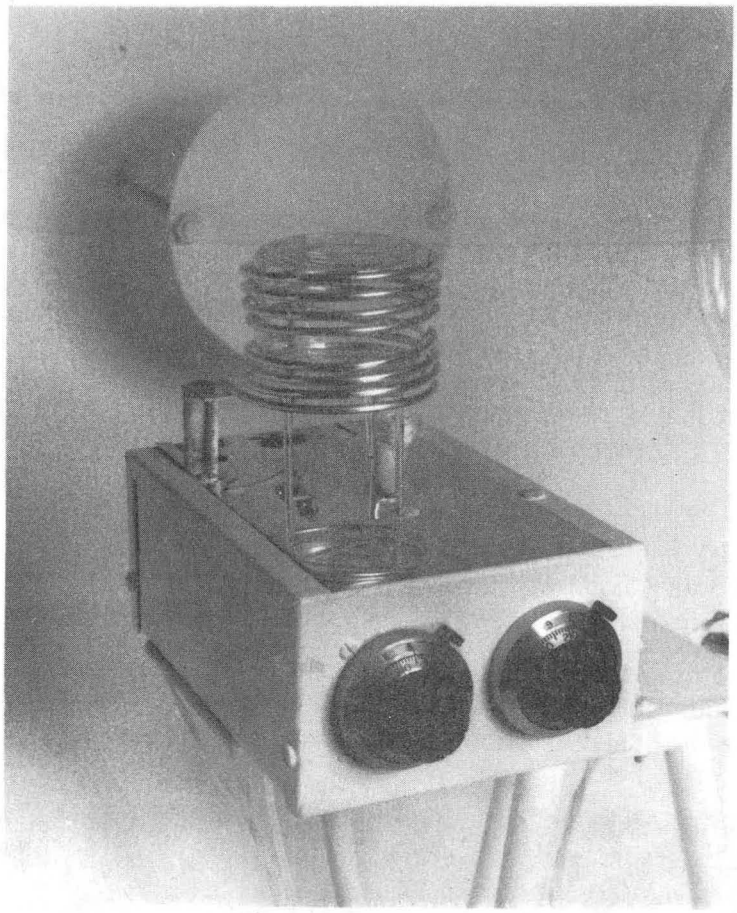

Figure 7b. Close-up of the electrodeless lamp. The arc envelope and outer container are supported on a narrow rod quartz tripod to allow maximum light release. Visual reflection of the coil, observed on the top of the matching network, is by a thin sheet of silver which serves to reduce eddy current loss and give good light reflection.

Table 4

CALCULATIONS FOR LAMP SL3

HIDSEF/LAMP 19-MAR-84 09:45:42

LAMP NO. = S.L.#3
GAS = NaI + TlI + Hg
PRESSURE = 2 ATMOS.

CONSTANTS:

SPHERE CALIBRATION	(LUMENS/mv)	315.40
MEAN DIA. OF SECONDARY	(cm)	3.90
CROSS SECT. DIA. OF SECONDARY	(cm)	0.50
COUPLING COEFFICIENT		0.32
REACTANCE OF PRIMARY	(Ohms)	306.28
RESONANT FREQ. OF PRIMARY	(MHz)	24.50
OPERATING FREQUENCY	(MHz)	13.56
VALUE OF SHUNT CAPACITOR	(pf)	360.00

Erms (V)	Irms (A)	ANG -LE	Itank (A)	PhDet (mv)	DSGPWR (W)	LUM -ENS	L/W	V/cm	W/cm	Rs	Cs (pf)	Itank (A)
244.9	2.72	+16.2	12.50	168.0	501.0	52987	106	12.3	40.9	3.6	28.3	12.20
245.3	2.27	+21.0	12.50	118.0	380.9	37217	98	12.2	31.1	4.8	28.4	12.15
249.7	3.10	+13.4	12.75	210.0	609.5	66234	109	12.6	49.7	3.1	28.3	12.50
260.2	3.89	+10.5	13.30	335.0	838.6	105659	126	13.2	68.4	2.5	28.2	13.12
263.7	3.84	+11.4	13.40	340.0	831.4	107236	129	13.4	67.9	2.6	28.2	13.25
276.3	4.54	+8.6	14.15	454.0	1061.1	143192	135	14.1	86.6	2.2	28.1	14.02

Table 5

CALCULATIONS FOR LAMP SL4

HIDSEF/LAMP 19-MAR-84 09:58:32

LAMP NO. = S.L.#4
GAS = Hg
PRESSURE = 3 ATMOS.

CONSTANTS:

SPHERE CALIBRATION	(LUMENS/mv)	315.40
MEAN DIA. OF SECONDARY	(cm)	3.90
CROSS SECT. DIA. OF SECONDARY	(cm)	0.50
COUPLING COEFFICIENT		0.32
REACTANCE OF PRIMARY	(Ohms)	306.28
RESONANT FREQ. OF PRIMARY	(MHz)	24.50
OPERATING FREQUENCY	(MHz)	13.56
VALUE OF SHUNT CAPACITOR	(pf)	360.00

Erms (V)	Irms (A)	ANG -LE	Itank (A)	PhDet (mv)	DSCPWR (W)	LUM -ENS	L/W	V/cm	W/cm	Rs	Cs (pf)	Itank (A)
322.4	2.30	+1.9	16.70	83.0	482.7	26178	54	16.7	39.4	7.0	28.3	16.54
322.5	2.57	-1.9	16.70	102.0	569.9	32171	56	16.8	46.5	6.0	28.2	16.66
323.0	2.85	-9.5	16.75	120.0	647.7	37848	58	17.1	52.9	5.5	28.1	16.93
325.6	3.29	-9.5	16.90	155.0	791.2	48887	62	17.3	64.6	4.6	28.1	17.14
326.1	2.01	+6.7	16.80	60.5	389.2	19082	49	16.7	31.8	8.8	28.3	16.62
329.8	3.89	-8.6	17.20	202.0	993.1	63711	64	17.5	81.1	3.8	28.1	17.41
342.2	4.40	+21.0	17.25	223.0	1128.4	70334	62	16.9	92.1	3.0	28.4	16.75

Table 6

CALCULATIONS FOR LAMP SL5

HIDSEF/LAMP 19-MAR-84 09:56:12

LAMP NO. = S.L.#5
GAS = TlI + Hg
PRESSURE = 2 ATMOS.

CONSTANTS:

SPHERE CALIBRATION	(LUMENS/mv)	315.40
MEAN DIA. OF SECONDARY	(cm)	3.90
CROSS SECT. DIA. OF SECONDARY	(cm)	0.60
COUPLING COEFFICIENT		0.32
REACTANCE OF PRIMARY	(Ohms)	306.28
RESONANT FREQ. OF PRIMARY	(MHz)	24.50
OPERATING FREQUENCY	(MHz)	13.56
VALUE OF SHUNT CAPACITOR	(pf)	360.00

Erms (V)	Irms (A)	ANG -LE	Itank (A)	PhDet (mv)	DSGPWR (W)	LUM -ENS	L/W	V/cm	W/cm	Rs	Cs (pf)	Itank (A)
216.5	2.49	-29.6	11.60	84.0	351.5	26494	75	11.6	28.7	4.6	27.9	11.94
217.3	2.68	-30.5	11.60	97.0	384.4	30594	80	11.7	31.4	4.3	27.9	12.07
217.5	2.94	-26.7	11.65	114.0	452.8	35956	79	11.7	37.0	3.7	27.9	12.08
217.6	2.25	-32.4	11.65	63.0	294.9	19870	67	11.6	24.1	5.6	27.9	11.96
219.6	3.34	-25.7	11.75	141.0	540.2	44471	82	11.9	44.1	3.2	27.8	12.30
222.2	3.73	-25.7	11.90	169.0	622.8	53303	86	12.2	50.8	2.9	27.8	12.57
225.4	4.19	-22.9	12.15	202.0	740.3	63711	86	12.4	60.4	2.5	27.7	12.79
229.2	4.83	-21.0	12.30	247.0	900.3	77904	87	12.7	73.5	2.1	27.6	13.13
231.2	5.14	-21.0	12.45	271.0	972.7	85473	88	12.9	79.4	2.0	27.6	13.32
233.7	5.54	-21.9	12.60	293.0	1061.0	92412	87	13.2	86.6	1.9	27.5	13.63
235.7	5.92	-20.0	12.75	322.0	1167.3	101559	87	13.3	95.3	1.8	27.5	13.76

Table 7

CALCULATIONS FOR LAMP SL7

HIDSEF/LAMP 19-MAR-84 09:49:13

LAMP NO. = S.L.#7
GAS = NaI + TlI + ScI3 + Hg
PRESSURE = 2.5 ATMOS.

CONSTANTS:

SPHERE CALIBRATION	(LUMENS/mv)	315.40
MEAN DIA. OF SECONDARY	(cm)	3.90
CROSS SECT. DIA. OF SECONDARY	(cm)	0.50
COUPLING COEFFICIENT		0.32
REACTANCE OF PRIMARY	(Ohms)	306.28
RESONANT FREQ. OF PRIMARY	(MHz)	24.50
OPERATING FREQUENCY	(MHz)	13.56
VALUE OF SHUNT CAPACITOR	(pf)	360.00

Erms (V)	Irms (A)	ANG -LE	Itank (A)	PhDet (mv)	DSGPWR (W)	LUM -ENS	L/W	V/cm	W/cm	Rs	Cs (pf)	Itank (A)
310.0	2.44	-28.6	16.25	142.0	420.5	44787	107	16.8	34.3	8.2	28.1	16.67
312.0	2.35	-23.8	16.30	145.0	424.6	45733	108	16.8	34.7	8.1	28.1	16.63
315.4	1.91	-7.6	16.30	120.0	352.2	37848	107	16.5	28.7	9.4	28.2	16.37
324.6	2.12	+1.9	16.75	155.0	427.6	48887	114	16.8	34.9	8.0	28.3	16.65
325.6	2.81	-16.2	16.90	242.0	612.4	76327	125	17.4	50.0	6.0	28.1	17.25
334.4	3.12	-13.4	17.30	304.0	734.5	95882	131	17.8	59.9	5.3	28.1	17.68
336.0	2.80	-4.8	17.30	266.0	657.9	83896	128	17.6	53.7	5.7	28.2	17.45
351.7	3.42	-7.6	18.25	380.0	878.2	119852	136	18.6	71.7	4.8	28.1	18.42

Table 8

CALCULATIONS FOR LAMP SL8

HIDSEF/LAMP 19-MAR-84 09:22:36

LAMP NO. = S.L.#8
GAS = NaI + TlI + Hg
PRESSURE = 2 ATMOS.

CONSTANTS:

SPHERE CALIBRATION	(LUMENS/mv)	315.40
MEAN DIA. OF SECONDARY	(cm)	3.90
CROSS SECT. DIA. OF SECONDARY	(cm)	0.50
COUPLING COEFFICIENT		0.32
REACTANCE OF PRIMARY	(Ohms)	306.28
RESONANT FREQ. OF PRIMARY	(MHz)	24.50
OPERATING FREQUENCY	(MHz)	13.56
VALUE OF SHUNT CAPACITOR	(pf)	360.00

Erms (V)	Irms (A)	ANG -LE	Itank (A)	PhDet (mv)	DSGPWR (W)	LUM -ENS	L/W	V/cm	W/cm	Rs	Cs (pf)	Itank (A)
241.9	2.32	-5.7	12.55	122.0	418.8	38479	92	12.7	34.2	4.7	28.2	12.63
242.2	2.30	-3.8	12.55	125.0	417.7	39425	94	12.7	34.1	4.7	28.2	12.60
245.7	2.71	0.0	12.70	180.4	523.6	56898	109	12.8	42.7	3.8	28.2	12.71
246.0	2.77	-2.9	12.75	188.0	535.6	59295	111	12.9	43.7	3.8	28.1	12.81
251.8	3.49	0.0	13.00	293.0	729.7	92412	127	13.2	59.6	2.9	28.1	13.09
252.4	3.54	0.0	13.00	299.0	743.6	94305	127	13.2	60.7	2.8	28.1	13.12
256.7	3.98	+1.0	13.25	377.0	864.6	118906	138	13.4	70.6	2.5	28.1	13.34
257.3	3.98	+1.0	13.25	372.0	866.2	117329	135	13.5	70.7	2.5	28.1	13.38
265.0	4.64	+1.0	13.70	465.0	1061.0	146661	138	13.9	86.6	2.2	28.0	13.83
266.5	4.64	+1.0	13.70	469.0	1068.7	147923	138	14.0	87.2	2.2	28.0	13.91

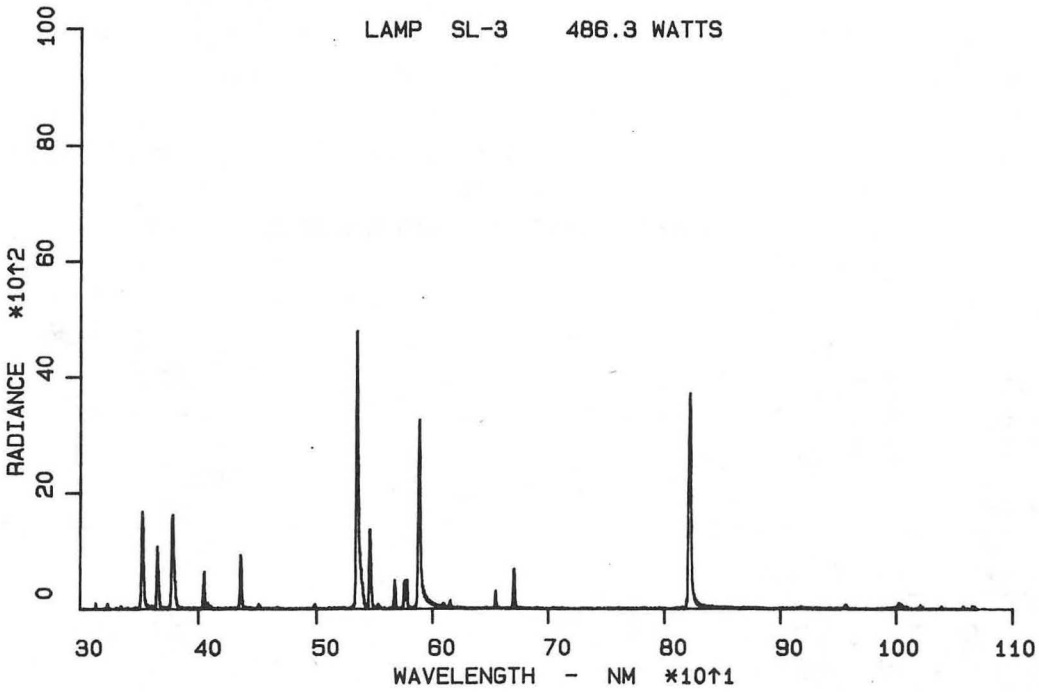

Figure 8. **Spectra of lamp SL3 at 486 W into the arc plasma. Ingredients were NaI (42 mg), TlI (5.4 mg), and mercury adequate to produce 2 atmospheres pressure when operating.**

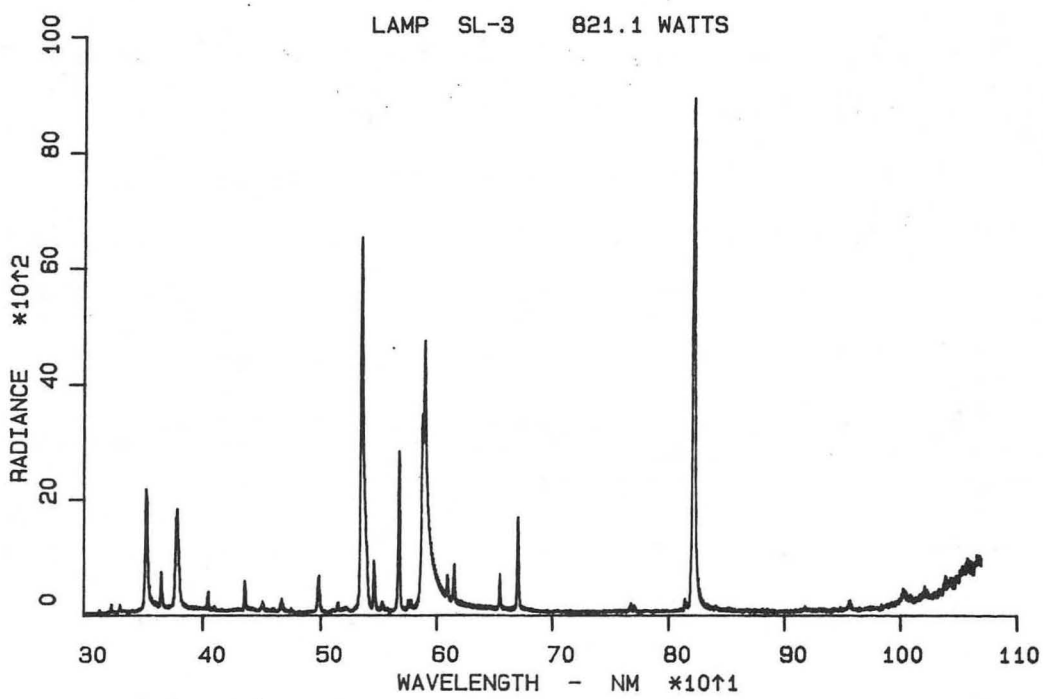

Figure 9. **Spectra of lamp SL3 at 821 W into the arc plasma. Ingredients were NaI (42 mg), TlI (5.4 mg), and mercury adequate to produce 2 atmospheres pressure when operating.**

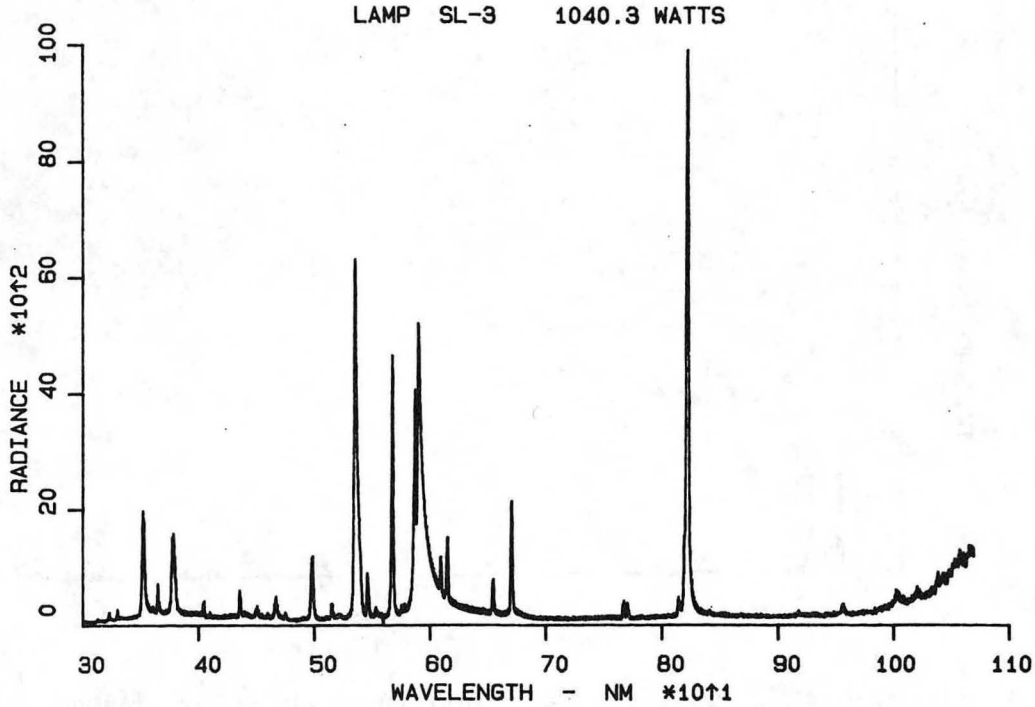

Figure 10. Spectra of lamp SL3 at 1040 W into the arc plasma. Ingredients were NaI (42 mg), TlI (5.4 mg), and mercury adequate to produce 2 atmospheres pressure when operating.

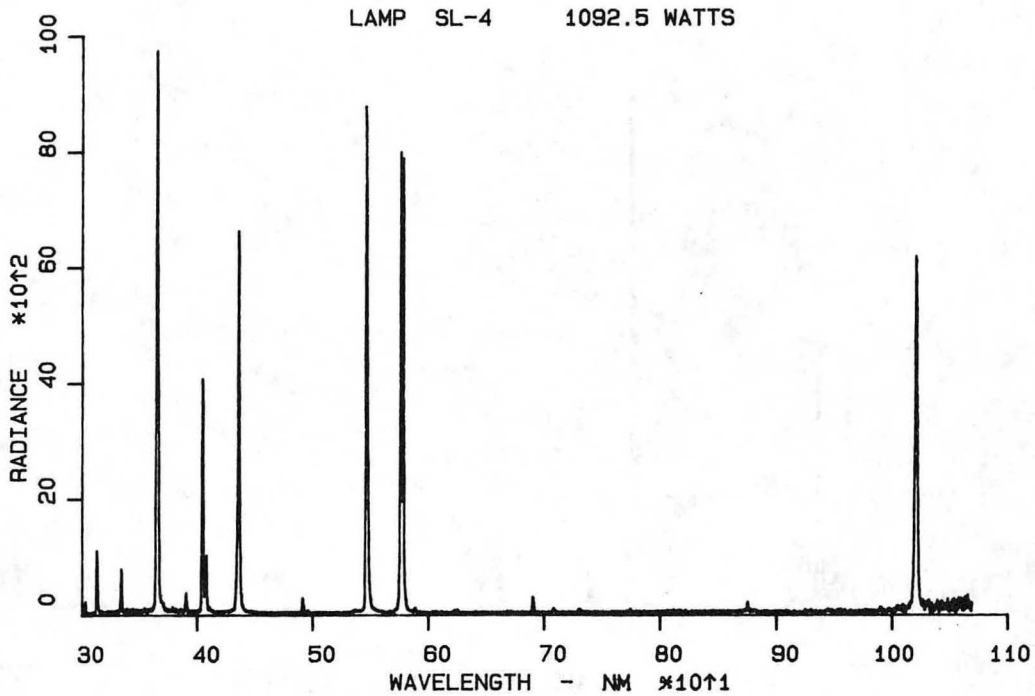

Figure 11. Spectra of lamp SL4 at 1092 W into the arc plasma. This lamp contained adequate mercury to produce 3 atmospheres pressure when operating.

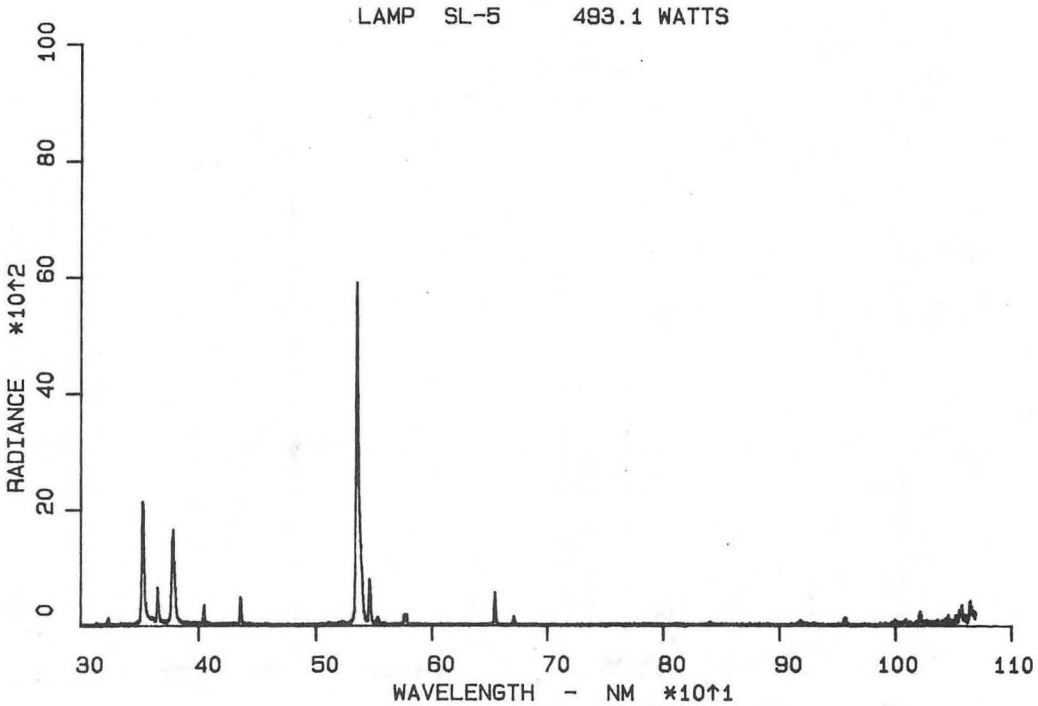

Figure 12. Spectra of lamp SL5 at 493 W into the arc plasma. Ingredients were TlI (1.7 mg), and mercury adequate to produce 2 atmospheres pressure when operating.

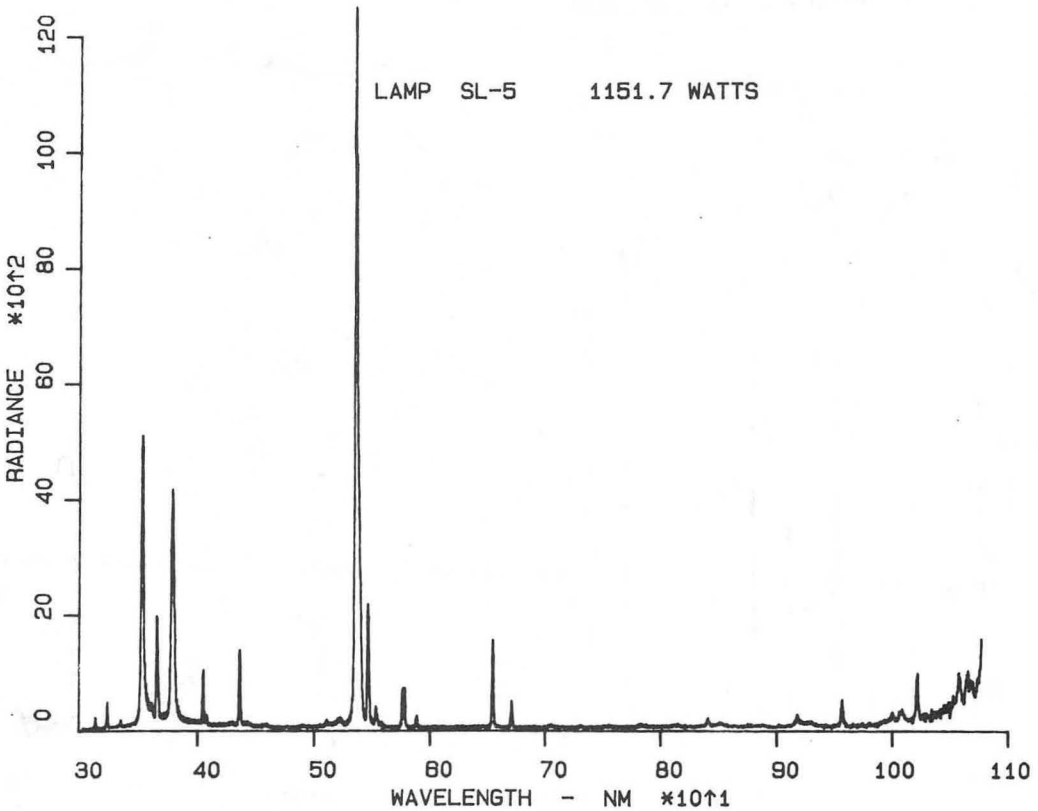

Figure 13. Spectra of lamp SL5 at 1151 W into the arc plasma. Ingredients were TlI (1.7 mg) and mercury adequate to produce 2 atmospheres pressure when operating.

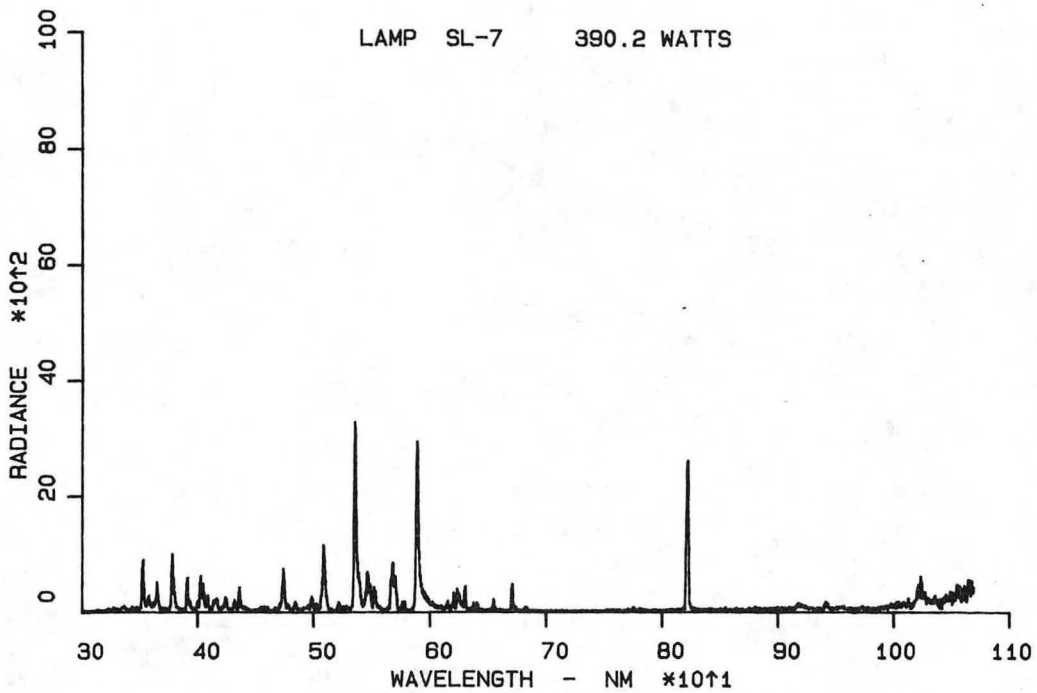

Figure 14. Spectra of lamp SL7 at 390 W into the arc plasma. Ingredients were NaI (42.6 mg), TlI (2.6 mg), ScI_3 (6.4 mg), and mercury adequate to produce 2.5 atmospheres pressure when operating.

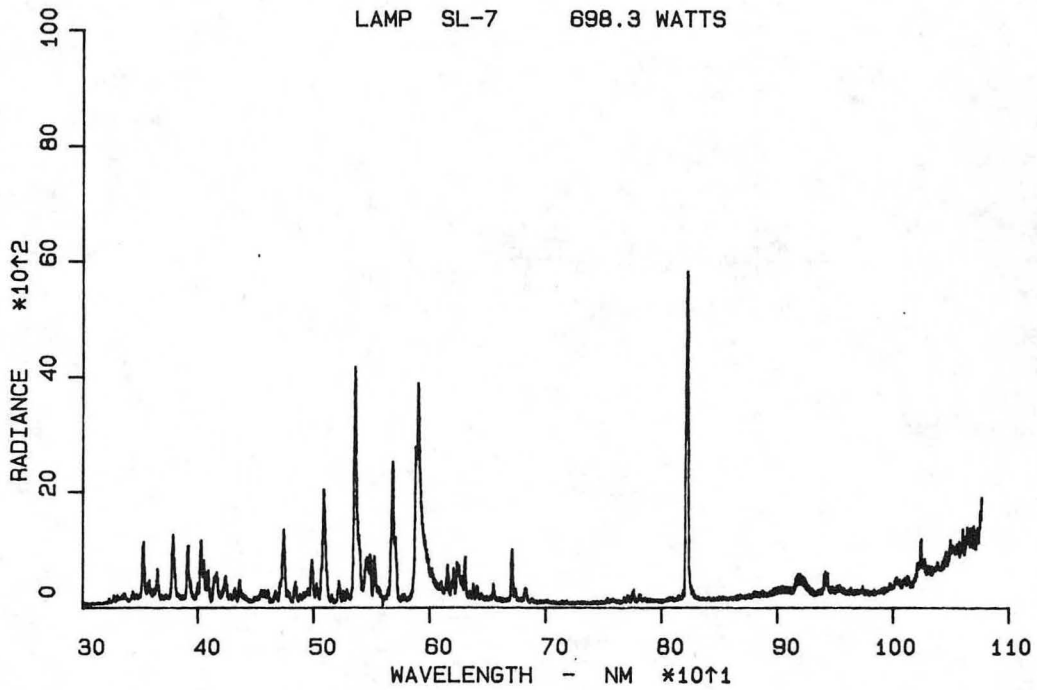

Figure 15. Spectra of lamp SL7 at 698 W into the arc plasma. Ingredients were NaI (42.6 mg), TlI (2.6 mg), ScI_3 (6.4 mg), and mercury adequate to produce 2.5 atmospheres pressure when operating.

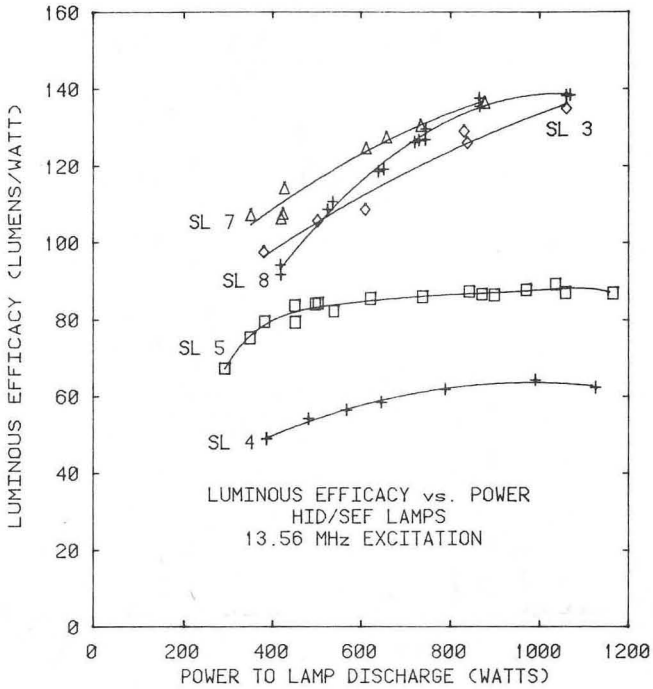

Figure 16. Measured efficacies of lamp SL3, 4, 5, 7, and 8 as a function of power delivered to the arc plasma. Lamp SL4 contains only mercury, permitting a firm comparison with well-established technology. Other lamps contain metal halides salts and generally agree with accepted performance of equivalent metal-halide HID lamps with electrodes.

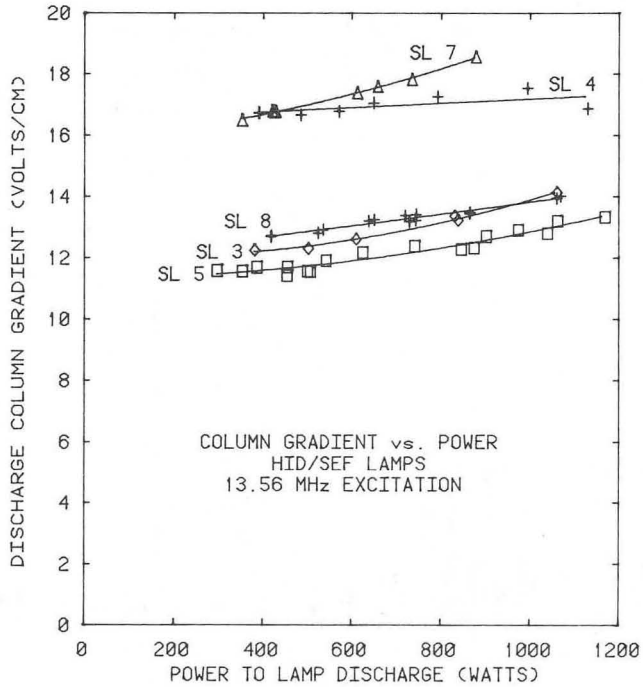

Figure 17. Calculated voltage gradient along the arc column (circumference of the arc ring) for various tested SEF/HID lamps. All curves show a mildly-positive V-I characteristic when the calculated arc current (Figure 18) is considered.

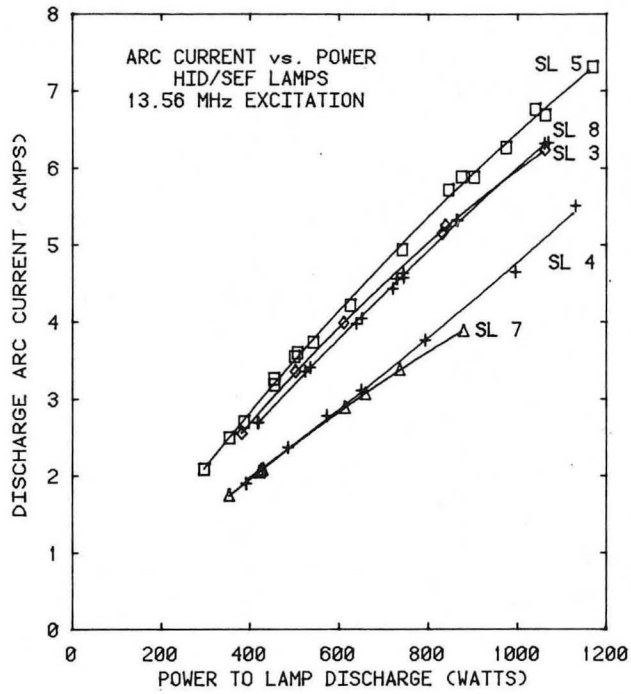

Figure 18. Calculated arc current for various SEF/HID lamps tested. The nearly proportional relation, with power to the arc plasma, is a reflection of the near-constant voltage gradient along the arc column (Figure 17).

Section 6

DISCUSSION

Efficacies measured in this study are presented in Figure 16 as a function of power transferred to the arc plasma. For the case of SL4, and for about 900 W input, the efficacy is close to 63 lm/W. It must be said that a strict comparison between the efficacy of the electrodeless lamp and the electroded lamp cannot be made because of the different geometries and thus the different thermal conditions in the two arc columns. Nevertheless these differences should not be enormous, and it is still instructive to make some comparisons. As shown in Appendix D, the skin depth at 13.56 MHz is adequate so that the electric field fully penetrates the plasma for all practical calculations. Thus, the excitation of the plasma is the same at 13.56 MHz as it is for dc or low power line frequencies, because the energy first goes to the free electrons of the plasma and they in turn transfer it to the various plasma processes independent of excitation frequency.

The conventional high pressure mercury lamp rated at 1000 W and used for roadway lighting, for example, has a distance between electrodes of 5.9 in. (15 cm). Its operating voltage, 265 V, minus about 12 V total electrode drop is 253 V, giving a column gradient of 16.87 V/cm. Referring to Figure 17 we see that the gradient measured in SL4 in our work at 900-1000 W input was ~ 17 V/cm. Both SL4 and the conventional 1000-W electroded mercury lamp have mercury doses such that the mercury pressure is about 3 atmospheres during operation. Now the electroded lamp with 1000 W input has about 50 W loss at the electrodes (4 A X 12 V). This subtracted from 1000 W give ~950 W into the column. The lamp gives ~57,000 initial lumens for a positive-column efficacy of 60 lm/W. We measure, under similiar power input, ~63 lm/W. Column loading is somewhat different for the two cases: 77.5 W/cm for the electrodeless lamp and 63.3 W/cm for the electroded lamp, but Figure 16 indicates that efficacy, for our case, is sensibly constant near 950 W input. The improvement in efficacy for the electrodeless lamp can perhaps be due to at least three factors:

1. The electrodeless lamp does not have an inner envelope wall which may, for its case, reduce heat loss by conduction from the column.
2. The end structure of the electroded lamp can lead to some light trapping, the exact value of which might be difficult to calculate.
3. The constriction of the arc column near the electrodes can possibly lead to regions of light production which are not as efficacious.

It is not known by the authors if the last effect has been subject to calculation in the past, but if not it might be worthy of study. Returning to point 1. above, the different geometry of the envelope wall for the electrodeless lamp raises the possibility that some of the energy lost to the walls in electroded lamps can be channeled to visible radiation; thus part of the higher efficacy we measure can be due to this cause.

A further comparison between the electrodeless and electroded arc can be made by referring to the work of Elenbaas, for instance page 149 of Reference 28. This comparison is more difficult to make because of different mercury dosing, wall diameter, etc., but in general Elenbaas does not indicate as high efficacy as we measure in this work, 63 lm/W compared to ~58 lm/W.

The spectra of all the arcs shown on Figure 8 through 15 are typical of the same ingredients in arc tubes with electrodes, and vary with power input (reservoir temperature) in the expected manner. Thus, it is unlikely that the greater efficacy comes about by any rearrangement of the spectra which might be peculiar to operation at 13.56 MHz. Rather, the improved efficacy is most probably due to the absence of end losses for light, found in conventional electroded arc envelopes, and the differences in arc and arc tube cross section geometry. The power loading of conventional mercury and mercury - metal halide arcs is generally 60 to 100 W/cm, corresponding to 700 to 1200 W in the electrodeless lamps.

The solenoidal excitation coil undoubtedly blocks and absorbs some of the emitted light. However, this is thought to be low. Well-polished silver reflects better than 98% of the light incident upon it. One or a few bounces on the coil surface and the photon escapes. It is exceedingly difficult to calculate these effects exactly, but light loss by the coil is probably only a few percent.

A unique difference between the electrodeless discharge tubes used for this work and conventional arc tubes is the difference in cross sectional geometry surrounding the arc column (ring) as noted above. Conventional arc tubes have cylindrical geometry and energy is lost by transport to the walls in all directions from the arc column. In the electrodeless configuration, direct energy transport to the walls occurs from about two-thirds of the circumference of the arc. The remaining one-third, in the direction of the center of the arc tube, of the energy escaping from the arc is dissipated in part by heating the gas adjacent to the arc column. In addition to retarding loss through thermal conduction, the geometry of the electrodeless arc envelope may give more radiation from low excitation energy species, because radiation is observed trailing away from the arc column toward the center of the envelope. In the case of the mercury arc, the excitation energy of the visible mercury lines is so high that this heating effect is inadequate to produce a diffuse inner arc boundary, but in metal halide arcs it can be readily observed.

The combined effects of elimination of end losses and reduction of wall losses provides a significant inherent efficacy advantage of the electrodeless arc tube configuration over conventional arc tubes with electrodes. The beneficial effects of reduction of wall losses can be maximized by using only arc ingredients with low excitation energies so that the arc core temperature is low and the arc has maximum diffuseness.

Figure 17 displays the electric gradient along the arc column as a function of power into the plasma. This is a calculated quantity because its direct measurement is near to impossible. Yet the gradients calculated are about that expected, and more easily measured, in electroded arcs. SL4 shows a high gradient because of the high mercury pressure, which reduces the electron mobility. SL5, 3, and 8 show lower gradients, principally because the mercury pressure is lower. Sodium and thallium iodides have low vapor pressures and contribute little to determination of the gradient. However, scandium iodide has a high vapor pressure, and dissociates to ScI and I_2 at a low enough gas temperature that the free iodine might increase the gradient by electron attachment along with some contraction of the current carrying channel of the arc. Lamp SL7, which has scandium iodide as one of its ingredients, shows about the same gradient as SL4. It is unfortunate that SL6 could not be started, because it also contained scandium iodide and would have been a good check.

Figure 18 presents the arc plasma current as a function of power input to the plasma for all lamps tested. The currents rise nearly linearily with power, a reflection of the near constancy of the arc voltage. Consideration of both Figures 17 and 18 shows that the arcs

are mildly positive in their V-I characteristics. This is expected on the basis, principally, of radiated energy loss, see page 171 of Reference 2. The electrical parameters of the arc present nothing unusual due to the 13.56 MHz operation. This is because the magnetic skin depth (see Appendix D) is long enough for the exciting electric field to be uniform throughout the arc.

Radiated spectra is shown on Figures 8 through 15 for SL3, 4, 5 and 7. Introduction of sodium, thallium and scandium iodides heavily suppresses the mercury spectrum as can be seen, as an example, for the 435.8 nm mercury line when Figures 9 and 11 are compared. In Figure 10 Sodium D lines are reversed. These and other features, discussed by Waymouth in Reference 2, are to be expected. All lamps show a portion of what may be thermal incandescence, beginning at ~1000 nm and extending to longer wavelengths. The origin of this is not certain at the present time.

Table 9 shows the relative radiated power of three of the arcs in the UV, visible, and near IR as determined from the spectra of Figures 10, 13, and 15. Also given are the efficacies and ICI color coordinates. The most significant comment which can be made from this comparison is that if the power input to the discharge, which emerges as radiative output from the plasma, could be confined to the visible, efficacies in excess of 200 l/W would be possible. Candidate radiative ingredients, which might approach this goal, have the low excitation energies, as described earlier, which may help to reduce wall losses as well.

Table 9

WAVELENGTH DISTRIBUTION OF OPTICAL ENERGY

Arc Tube		Wavelength Range (nm)				l/W	X	Y
		300-400	400-700	700-1000	300-1000			
SL-3	1040W	0.109	0.566	0.325	1.00	135	.469	.425
SL-5	1152W	0.291	0.516	0.193	1.00	87		
SL-7	698W	0.106	0.564	0.330	1.00	131	.394	.428

Section 7

CONCLUSIONS AND RECOMMENDATIONS FOR FUTURE WORK

High intensity discharge lamps were successfully excited by solenoidal electric fields in the range from about 400 to 1000 W. Frequency of operation was 13.56 MHz in the ISM (Industrial, Medical, and Scientific) band. Quartz discharge envelopes were filled with various combinations of mercury, sodium iodide, thallium iodide, and scandium iodide, and efficacies measured were essentially those expected as based upon the positive column efficacies of conventional metal halide lamps. The arc plasma was stable and had the appearance of dc or 60 Hz arc columns. Calculated skin depth at 13.56 MHz is adequate to assure uniform electric field across the column, accounting for the similarity to dc arcs.

During this program, equipment was designed and built (Appendix C) that allowed an accurate measurement of electrical power to the lamp assembly at 13.56 MHz. Electrical quantities were calculated from an equivalent circuit that, in particular, took account of the stray capacity across the solenoidal excitation coil. Current in this coil was typically $\sim$15 A and voltage across eight turns was therefore $\sim$5000 V because coil reactance was 300 Ω. The high impedance of the coil was approximately matched to a 50-Ω transmission line by a capacitive matching network. The lamps started in a low plasma resistance mode and moved to high resistance as the mercury vapor increased. There was considerable mismatch during starting and warm up, but under final operating conditions the lamp plasma could be matched overall to the power source. Power loss in the coil was high, however. It was $\sim$100 W or more, and when included in a calculation of efficacy, reduces the overall system efficacy considerably. More work will be required to reduce the current in the excitation coil by increasing the coupling coefficient between the coil and the lamp plasma ring, either by changes in geometry or partial use of ferrite material. Difficulty was encountered getting into the solenoidal mode of operation. This can be reduced by development of more voltage through changes in the coil and magnetic path, again by better design.

Also, from the standpoint of heat management, the arc envelope should receive attention to balance the reservoir temperature for halide salts, and allow closer proximity of the excitation coil. Most lamps show greater efficacy as the power to the arc envelope increases (greater halide vapor pressure). If future emphasis is on lower power lamps, the arc envelope, and thus the diameter of the arc ring, can be reduced while maintaining the same power loading of the column. There is some limit to how far this can be continued and still get sufficient magnetic flux in the ring to give the necessary voltage gradient. This should be investigated in future work.

We have found the expected efficacies in lamps containing conventional ingredients. These ingredients are chosen in metal vapor lamps to allow long life of the electrodes. Without electrodes, the SEF/HID lamp is not so restrained, and a program to find unconventional gas fills, which might give greater efficacies, should be conducted. The construction of the necessary equipment and its successful operation during the current program should provide an excellent introduction into a second program where the efficacies of unconventional fills would be tested.

Finally, even though good efficacies with stable operation are indicated in this work, there will need to be a considerable effort to design a practical ballast/matching network/coil/lamp assembly with emphasis on mechanical ruggedness, heat management, electrical efficiency, and good light release and control. EMI and hazards to safety are most probably controllable but must be regarded.

Section 8

REFERENCES

[1] Jack A.G. and Koedam M., *Journal of I.E.S., 3, 323* (1974).

[2] Waymouth, J.F., *Electric Discharge Lamps,* The M.I.T. Press, Cambridge (1971)

[3] Grabner, H. and Pilz, W., "High Pressure Discharge in Metal Vapor with High Visual Efficiency," *Eight Int. Conf. on Phenomena in Ionized Gases,* paper 3.2.6.6, p 228 (1967).

[4] Morrison, M., Mercury Vapor Lamp, U.S. patent 1,813,580 (1931).

[5] Morrison, M., Mercury Vapor Lamp, U.S. patent 1,807,927 (1931).

[6] Babat, G.I., *Inst. Elec. Eng. (London), vol 94,* pp 27-37 (1947).

[7] Eckert, H.V., *High Temperature Science, vol 6,* p. 99 (1974)

[8] Hollister, D.D., "High Pressure Method for Producing an Electrodeless Plasma Arc as a Light Source," U.S. patent 3,763,392 (1973).

[9] Hollister, D.D., "Method for Using Metallic Halides for Light Production in Electrodeless Lamps," U.S. patent 3,860,854 (1975).

[10] Yamamoto, M., "Circular-Shaped Induction Discharging Light-Emitter Tubes," Japanese patent 36257/70 (1970).

[11] Haugsjaa, P.O., et al, "Electrodeless Light Source Having a Lamp Holding Fixture Which Has a Separate Characteristic Impedance for the Lamp Starting and Operating Mode," U.S. patent 3,943,401 (1976).

[12] Haugsjaa, P.O., et al, "Termination Fixture for an Electrodeless Lamp," U.S. patent 3,943,402 (1976).

[13] Haugsjaa, P.O., et al, "Electrodeless Light Source Utilizing a Lamp Termination Fixture Having Parallel Capacitive Impedance Matching Capability," U.S. patent 3,943,403 (1976).

[14] McNeill, W.H., et al, "Helical Couplers for Use in an Electrodeless Light Source," U.S. patent 3,943,404 (1976).

[15] Anderson, J.M., "High Frequency Electrodeless Fluorescent Lamp Assembly," U.S. patent 3,521,120 (1970).

[16] Anderson, J.M., "Electrodeless Fluorescent Lamp Having a Radio Frequency Gas Discharge Excited by a Closed Loop Magnetic Core," U.S. patent 4,017,764 (1977).

[17] Anderson, J.M., and Johnson, P.D., "Helical Wire Coil in Solenoidal Lamp Tip-Off Region Wetted by Alloy Forming an Amalgam with Mercury," U.S. patent 4,262,231 (1981).

[18] Anderson, J.M., "Electrodeless Gaseous Electric Discharge Devices Utilizing Ferrite Cores," U.S. patent 3,500,118 (1970).

[19] Anderson, J.M., "High Intensity Discharge Lamp Geometries," U.S. patent 4,180,763 (1979).

[20] Grover, F.W., *Inductance Calculations,* D. VanNostrand Company, 1946.

[21] Terman, F.E., *Radio Engineers Handbook,* McGraw-Hill Book Company, 1943.

[22] Langford-Smith F., *Radiotron Designers Handbook,* Amalgamated Wireless Valve Co., Sydney Australia, 1953, 4th Edition. Reproduced and distributed by Radio Corporation of America, Harrison, N.J.

[23] Butterworth S., "Effective Resistance of Inductance Coils at Radio Frequencies," *The Wireless Engineer, 3,* pp 203-10, pp 309-16, pp 417-24, pp 483-92 (1926), Also, *Proc Royal Soc (L), 107,* pp 693-715 (1925).

[24] Medhurst R.G., "H.F. Resistance and Self-Capacitance of Single-Layer Solenoid," *The Wireless Engineer, 24,* pp 35-43, pp 80-92 (1947).

[25] Sekiguchi T. and Herndon R.C., "The Thermal Conductivity of an Electron Gas in a Gaseous Plasma," *Phys. Rev, 112,* p 1 (1958).

[26] Grover F.W., *Inductance Calculations,* D. Van Nostrand Company, Inc., New York, 1946.

[27] Anderson J.M., "Temperature Determination in High-Pressure Sodium Discharges by Detection of RF Thermal Noise," *Jour. Appl. Phys, 46,* p 1531-34 (1975).

[28] Elenbaas, W., *The High Pressure Mercury Vapor Discharge,* North Holland Publishing Co., Amsterdam 1951.

[29] Johnk, C.T.A., *Engineering Electromagnetic Fields and Waves,* John Wiley and Sons, New York, 1975.

[30] Stratton, J.A., *Electromagnetic Theory,* McGraw Hill Book Co, First Edition, 1941.

Appendix A

DETERMINATION OF THE COUPLING COEFFICIENT BY BRIDGE MEASUREMENTS

Input impedance to a two-loop circuit, with magnetic coupling between the loops, is obtainable from text books,

$$Z_{in} = R_p + j\, wL_p + k^2\, (wL_p)(wL_s)\, X \left[\frac{R_s}{R_s^2 + (wL_s)^2} - j\, \frac{wL_s}{R_s^2 + (wL_s)^2} \right] \tag{A-1}$$

where,

R_p is the primary resistance

R_s is the secondary resistance

wL_p is the primary reactance

wL_s is the secondary reactance, and

k is the coupling coefficient.

Resistive and reactive components of impedance are reflected from the secondary (second loop) into the primary circuit according to the factor k^2. If k=1, and if wL_p and wL_s are large with respect to primary and secondary resistances, the case of the ideal transformer is recovered, giving an input resistance equal to $R_p + R_s\ (L_p\ /\ L_s)$. The lamps described in this report are excited by a transformer core which is either partly air (ferrite complemented), or completely air core. The coupling coefficient is thus generally less than unity, due to stray flux which is not mutual to both loops. The reflected resistance and reactance, second term of A-1, take on a more complex variation with R_s as shown schematically on Figure 4. One notes that the reflected resistance peaks, at nearly $R_s = wL_s$, while the reactance acts to reduce the primary inductive reactance, according to A-1, especially at low values of R_s. Passing to the limit of $R_s = 0$, the resistive component disappears and the reflected reactance is described only by the values of wL_p and wL_s. If these, as well as the resulting reduction in the reactive component of the input impedance, are measured or calculated, the value of k is determined. Experimentally, the procedure is to alternately place a short-circuited metal ring ($R_s << wL_s$) in the space, which would be ultimately occupied by the discharge plasma, and note the change in input reactance.

Returning to the reflected resistance, it should be clear that the primary current, passing through this resistance, determines the magnitude of power delivered to R_s. If the secondary is a ring of plasma, in our case the SEF lamp, $I_p^2\ R_r$ is the power delivered to the plasma. R_r is the reflected resistance. One should attempt in a final design to operate as near to the peak of the R_r curve on Figure 4 as possible. This reduces the primary current necessary for transfer of the desired power, which in turn improves the overall efficiency by minimizing power loss in R_p.

Initial measurements of electrical quantities in the SEF/HID lamp and coupling circuit were made with a magnetic core partly of type Q-1 ferrite material made by Indiana Gen-

eral Company. The geometry is sketched on Figure 1. Input impedance was measured with a General Radio Model 1606A Bridge at 13.56 MHz. To determine the coupling coefficient, a short-circuited secondary in the form of a short thin-wall copper cylinder 5 cm in diameter and 1.2 cm high was placed in a six-turn primary coil. Its calculated inductance was 0.0531 μH.[20,21] The primary, wound of 1/8-in. (0.317 cm) copper tubing, was 8 cm in diameter and 4.5 cm high. The toroidal ferrite cores were cut and arranged as shown on Figure 2. They were part numbers F-1824-1-21Q-1 with size O.D. 14.57 cm, I.D. 6.24 cm, and thickness 1.53 cm obtained from Permag Corporation, Jamaica, New York. The bridge-measured input reactance to this arrangement was 416 Ω. With the shorted secondary in place, the reactance was 320.8 Ω, giving k=.478 and k^2 = 0.229. Ferrite cores were not used in our final measurements and so the arrangement of Figure 2 will not be further discussed.

Instead, an air core transformer was used with a coil as shown on Figure 3. Copper tubing with the same cross sectional diameter, 0.317 cm, was used to wind an eight turn coil 5.1 cm high and 6.35 cm inner coil diameter. The coil was expanded somewhat in its center, 0.95 cm, to form two, four-turn spaced coils. The shorted secondary was also a short cylinder of copper with diameter 3.7 cm and height 0.75 cm. Its calculated inductance was 0.0940 μH so that wL_s = 8.01 Ω at 13.56 MHz. Bridge readings after silver plating were:

Z in = 0.45 + j 363.6 Ω w/o secondary

Z in = 0.45 + j 327.1 Ω w/ secondary

to give k = 0.317 and k^2 = 0.10

This coil reactance, 363.6 Ω, is somewhat higher than one would have calculated using inductance formulas, namely about 306 Ω, the difference being attributable to stray capacity between coil winding as discussed in another section of this report. Also, the coupling coefficient is considerably less than that with partial use of ferrites in the magnetic path.

Appendix B

SOME COMMENTS ON PRIMARY COIL DESIGN

Until such frequencies are reached that the current in the turns of a coil can no longer be reasonably regarded to be in phase throughout the coil, the inductance of the coil can be well approximated by that calculated at low frequencies or dc. Standard formulas are readily available [20] and a good overall summary can be found in Terman.[21] The following expression [22] has been found to be useful in computer calculations.

$$L_o = RN \frac{RN}{\left[9 - \left(\frac{R}{5\,L}\right)\right] R + 10\,L} - 0.0319 \left[2.3 \log_{10} \left(1.73 \frac{Nd}{L}\right) + 0.336 \left(1 - \frac{2.5}{N} + \frac{3.8}{N^2}\right)\right] \tag{B-1}$$

microhenries, where

R = coil radius to center of wire, inches

N = number of turns

L = coil length, inches

d = wire diameter, inches.

Two other parameters of solenoidal single-layer coils are of importance to us: the RF resistance and the self capacity. The former can be much greater than the dc resistance of the coil, leading to power loss, and the latter has the effect of increasing both the apparent RF resistance and the inductive reactance over that calculated.

The RF resistance of a coil is due to two factors. The first is the increase, with frequency, in resistance of only the wire, as would be the case if the wire were stretched straight.[21] The second is a result of coiling the wire. Eddy currents in each turn, as a result of the magnetic field from the other turns, further redistributes the current, increasing the resistance. A rather comprehensive work by Butterworth [23] was the first to study the problem in detail, but the definitive papers were written by Medhurst in 1947.[24] The results of these papers cannot be placed into a simple analytic expression but rather must be approximated by curves which ultimately give the RF resistance with enough accuracy for practical purposes. Toward this end, Tables VIII and IX on page 88 of [24] are helpful.

A major contribution of Medhurst's was to clarify the literature with respect to the self capacity of coils. His result, if one end of the coil is at ground potential, is

$$C = D \left(0.1126 \frac{l}{D} + 0.08 + 0.27 \left(\frac{l}{D}\right)^{-1/2}\right) \tag{B-2}$$

where C is in pF

D = coil diameter in cm

l = coil length in cm

After calculation of coil RF resistance and inductive reactance the apparent impedance which the coil presents to the circuit into which it is placed is typically greater than calculated. The reason for this is that the stray coil capacity, which includes lead capacity, tends to resonate the coil somewhat, even though the self-resonant frequency of the coil may be considerably above the operating frequency. Table 2 shows a printout of calculated quantities as a function of frequency of operation. The coil is eight turns of No.8 copper wire with mean diameter 2.6 in. (6.6 cm) and height 1.8 in. (4.57 cm). Note that the self-resonant frequency is 30.3 MHz. For this particular example the leads were taken 4.5 in. long and spaced 0.5 in. The coil self-capacity alone calculates, from Equation B-2, to 3.18 pF while the printout indicates a total of 7.67 pF because it includes the lead capacity. It is interesting that the dc resistance is only 0.00382 Ω while the R_{ac} at 13.56 MHz is 0.279 Ω, a factor of 73 larger. The calculated inductance of this coil is 3.595 μH, giving 306.3 Ω of inductive reactance at 13.56 MHz. However, the R_{in} and X_{in} calculate to 0.436 and 386.8 Ω, respectively. The increase is due to the stray capacity as indicated above and is calculable from, [21]

$$L\ (apparent) = L\ (low\ frequency)\ (1 - (f/f_r)^2)^{-1} \tag{B-3}$$

$$R_{ac}\ (apparent) = R_{ac}\ (calculated)\ (1 - (f/f_r)^2)^{-2} \tag{B-4}$$

where f is the operating frequency and f_r is the self-resonant frequency.

Figure 19 given the results of calculations (13.56 MHz) for coils with various wire sizes. To keep good spacing between turns, the air gap was held to 0.1 in. (0.254 cm). One can see that the R_{ac} decreases with increasing wire diameter, as might be expected. This curve typically can have a minimum; for too large wire diameters the loss goes up again. We are not in that range on Figure 19, but the 8-gauge wire we have chosen for the experiment gives a quite low R_{ac} compared to smaller wire diameters. Apparent coil resistance and reactance (from Equations B-3 and B-4) also fall with larger wire diameters.

The RF resistance of the primary coil is of considerable importance for overall lamp efficacy. In some of the lamps we have operated, the primary coil current needed to be about 16 A for generation of the voltage to maintain the lamp. The power loss in the coil was then 71 W if the RF resistance is taken as 0.28 Ω. In practice the loss was higher. At the 400 W level this represents a drop to 82% efficiency. We have used water cooling of the coil. In practice this might not be practical, meaning that the coil would operate at a higher temperature and give correspondingly more loss. As an example, if the conditions for Table 2 were kept the same except that the wire temperature was raised to 500 °C, the RF resistance would increase from 0.279 Ω at 25°C to 0.441, a factor of 1.58. Figure b shows that the apparent resistance would move to 0.67 Ω. Silver plating the coil decreases the resistance only little, its main advantage being a reduction of oxidation and better reflection of light. A polished silver surface reflects about 98% through the visible range. Location of the coil near the plasma reduces the efficacy much less than might be at first suspected, because multiple reflections eventually release the light.

Changing coil height, while keeping the wire diameter constant, has a strong effect on resistance. The apparent resistance is shown on Figure 20. We chose to operate with a coil which was about 1.8 in. tall and had an apparent resistance of 0.43 Ω. Expanding the coil to greater height would have reduced loss, but the coupling coefficient would also reduce because some turns would then be further from the lamp plasma.

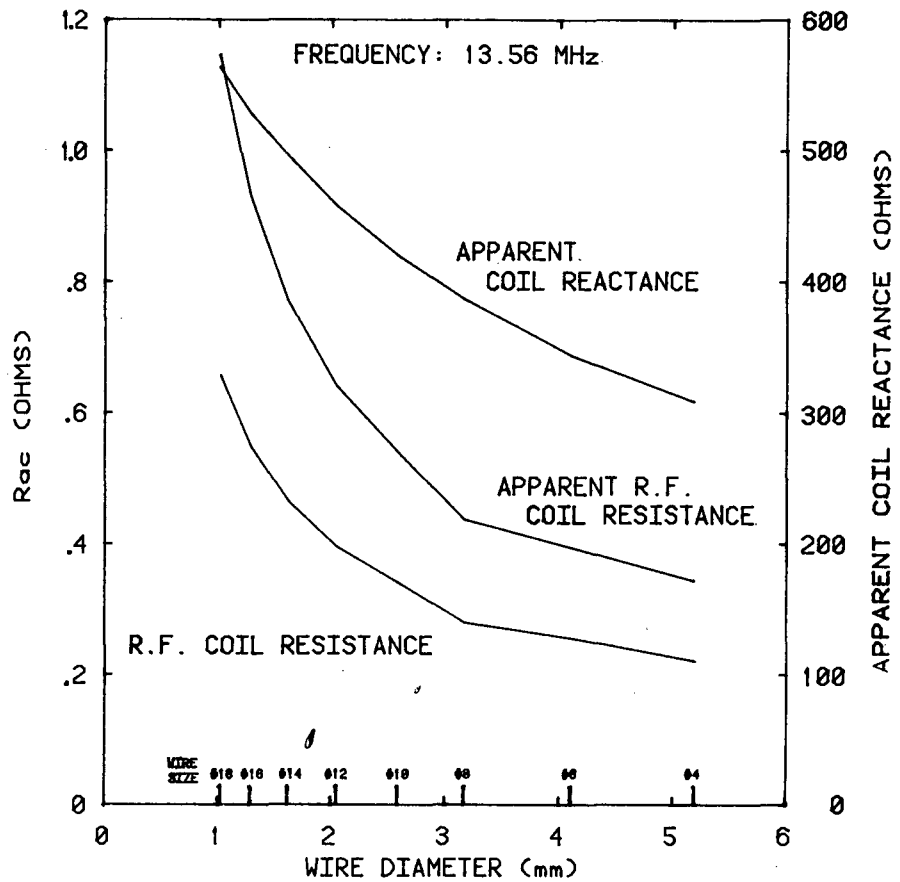

Figure 19. RF resistance of a solenoidal coil of wire (lowest curve) as the wire diameter is varied. Spacing between turns (air gap) is held at 0.1 in. (0.25 cm) to provide adequate voltage withstand. Apparent input resistance and reactance are calculated by including the stray capacity of the coil and leads. Frequency is 13.56 MHz. All quantities are calculated.

The voltage applied to the HID lamp plasma in this work ranged up to ~200 V. This volts/turn must be developed by current in the primary coil. Take the coupling coefficient at ~0.3 and assume that this number represents approximately the fraction of flux from the primary which engages the secondary plasma ring. Thus, we must develop 200/0.3 = 667 V per turn in the primary coil. If there are eight turns in the primary, the total primary voltage is approximately 5.3 kV (rms). The calculated primary reactance is 306 Ω, as noted earlier, and thus primary current must be 17.4 A to give finally a discharge voltage of 200 V/turn. The consequence of this result, aside from the fact that such high currents lead to power loss in the coil, is that the primary voltage is high. Handling this voltage without arc-over becomes a concern, especially if the coil must be supplied with water through tubing for cooling. We have found that common forms of plastic tubing will not suffice due to dielectric heating at the high voltage end of the coil. Teflon tubing, kept cool by water flow, appears to work quite well. Power loss in both the Teflon and the water appears to be small in so far as can be determined. The Teflon tubing used in this

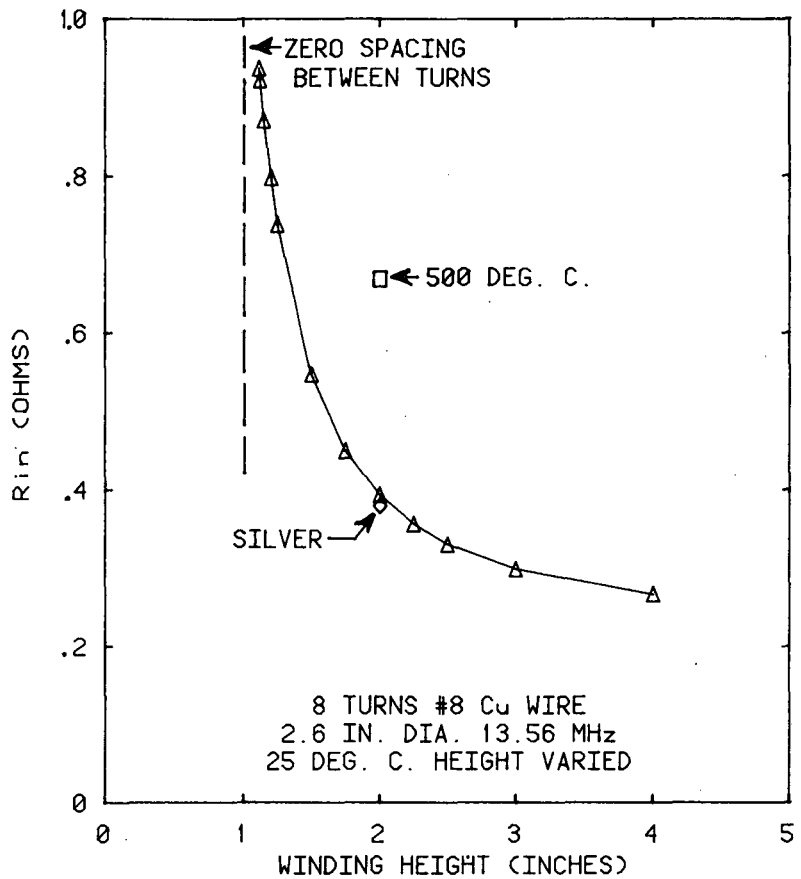

Figure 20. Input resistance to a solenoidal coil of wire (No.8 gauge) as the height of the coil is varied. Silver wire or silver-plating makes very little reduction in resistance, as the comparison at 2 in. height indicates. Higher wire temperature, 500°C, makes a considerable increase of resistance for the copper wire coil. All quantities are calculated.

work had an inner diameter of about 2.5 mm and a wall thickness of about 1 mm. Water flow was typically 300 ml/minute, and current transformers showed that no measurable RF current flowed down the water line after a few centimeters from the point of attachment to the coil. Tap water was used. Power loss in the coil due to RF resistance can be measured by monitoring the temperature difference between water into and water from the coil.

Support of the primary coil high voltage terminal must be done with insulating material which does not induce flashover. Good quality steatite ceramics or quartz can be used for rigidity but the path length to ground potential must be several centimeters. Charge buildup on the insulator surface aids breakdown much as would be the case for dielectric-covered electrodes. Teflon, while it has low bulk loss at 13.56 MHz, has poor surface resistance to breakdown, and once arced, loses its voltage withstand ability until cleaned of arc products. The best insulator is air with rounded metal electrodes and this suggests

that in any final practical design the high voltage end of the coil should be supported directly on the end terminal of the series matching capacitor. Any insulators should be protected by rounded metal surfaces to relieve stress at metal/insulator interfaces. Breakdown between coil turns occurred only once in our work but the effect was to badly damage the silver plating and reduce the light escaping from the lamp. Maintenance of about 0.10 in. (0.25 cm) between the turns appears adequate to prevent this.

Before leaving the discussion of the primary coil design, we should comment on a question which may arise; Will a coil of the dimensions used here radiate appreciable power at 13.56 MHz? We find the power radiated from a current loop (Reference 30, page 438) to be

$$W = 160\, \pi^6 \left(\frac{R}{\lambda}\right)^4 I_o^2 \tag{B-5}$$

where R is the radius of the current loop, λ is the free space wavelength, and I_o is the maximum of the alternating current in the loop. For our case, R is 3.5 cm, λ is 2212 cm, and the highest value of I_o to be expected in our experiment, is (20)(1.414)(number of turns) = 226 A peak. This is eight turns at 20 rms A/turn. From the above expression the calculated power in the far field becomes 0.049 W. This value is negligible when levels of 400 to 1000 W are being considered, and it does not enter into the efficacy calculations.

Appendix C

DESIGN AND CALIBRATION OF THE POWER MEASURING EQUIPMENT

To enable measurement of lamp voltage, current, and power we designed and constructed a voltage and current pickoff assembly. The probable range of currents to be measured was expected to be from 0.1 to 10 A, with the voltage range from 1 to 500 V. A current transformer was chosen for minimum perturbation of the line impedance. A capacitive voltage divider was chosen also for fidelity and minimum disturbance. The current transformer consisted of 50 turns of No.18 magnet wire on a ferrite core (OD, 3.25 cm; ID, 1.93 cm; thickness, 0.96 cm) of Q-1 material (Indiana General). The transformer operated into a 50-Ω line, terminated at a Tektronix 7854 Digital oscilloscope and had an overall transfer ratio of 1 V/A. The capacitive divider, with a ratio of 1000:1, was designed for an input capacity of 2.35 pF and a output capacity of 2350 pF. It also operated into a 50 Ω line terminated at the oscilloscope. Both sensors were housed in a single machined case for stability. A sketch of the setup is given on Figure 21. Connectors on the line carrying power from the source to the lamp were type HN and connectors carrying the sensed current and voltage were type N. Ferrite cores on all the lines reduced conducted currents and other interferences.

The calibration of the sensors and the overall setup will be described in detail later, but for the moment let it be said that the power source and water load, Model 8720 obtained from Bird Electronic Corporation, Cleveland, Ohio, were operated up to one kilowatt, and the true power measured by water temperature difference at a known flow rate. If the load resistance is known (51.05 Ω), both line current and line voltage can be calculated. Using the water load, we determined that the current transformer output was 7% too low and voltage pick off, 13% too high. These could be corrected by mechanical alteration, but we chose to add correction factors to the program in the oscilloscope to provide a correct power calculation. Phase shift between voltage and current was a few degrees and was corrected by changing the length of the cables between the sensors and the oscilloscope. A change of a few inches was sufficient to eliminate the phase error.

The Tektronix 7854 digital oscilloscope was used to calculate power delivered to the lamp. A program was written and stored in the oscilloscope which acquired the voltage and current waveforms, digitally multiplied them, and calculated average power.

A considerable effort was expended to calibrate the R.F. power measuring equipment at 13.56 MHz. Commercially available power meters at this frequency are of the bolometer/thermistor type or the E-H coaxial pickoff type. Both suffer from various errors, and after some considerable expense, the accuracy may be ~1% of full scale. An alternate approach is to use low frequency instruments which are more accurate, and to reference them to the higher frequency. The low frequency instrument used was a Transfer Standard Sensitive Research single phase wattmeter Model DW, Serial No. ES-5217, accuracy 0.25% of full scale.

The scheme of calibration involved two paths from 60 Hz to 13.56 MHz. On the one hand, a water-cooled coaxial load, Bird Model 8720, was operated at both 60 Hz and 13.56 MHz. It was assumed that the load resistance remained the same at both frequencies. At 60 Hz, the Model DW wattmeter measured the input power at levels up to about 400 W. After the water-cooled load was calibrated, it was used to calibrate our power measuring set up. Secondly, the same Model DW wattmeter was used to measure power to a 1000-W tungsten projection lamp, type DRB, located in the light integrating sphere.

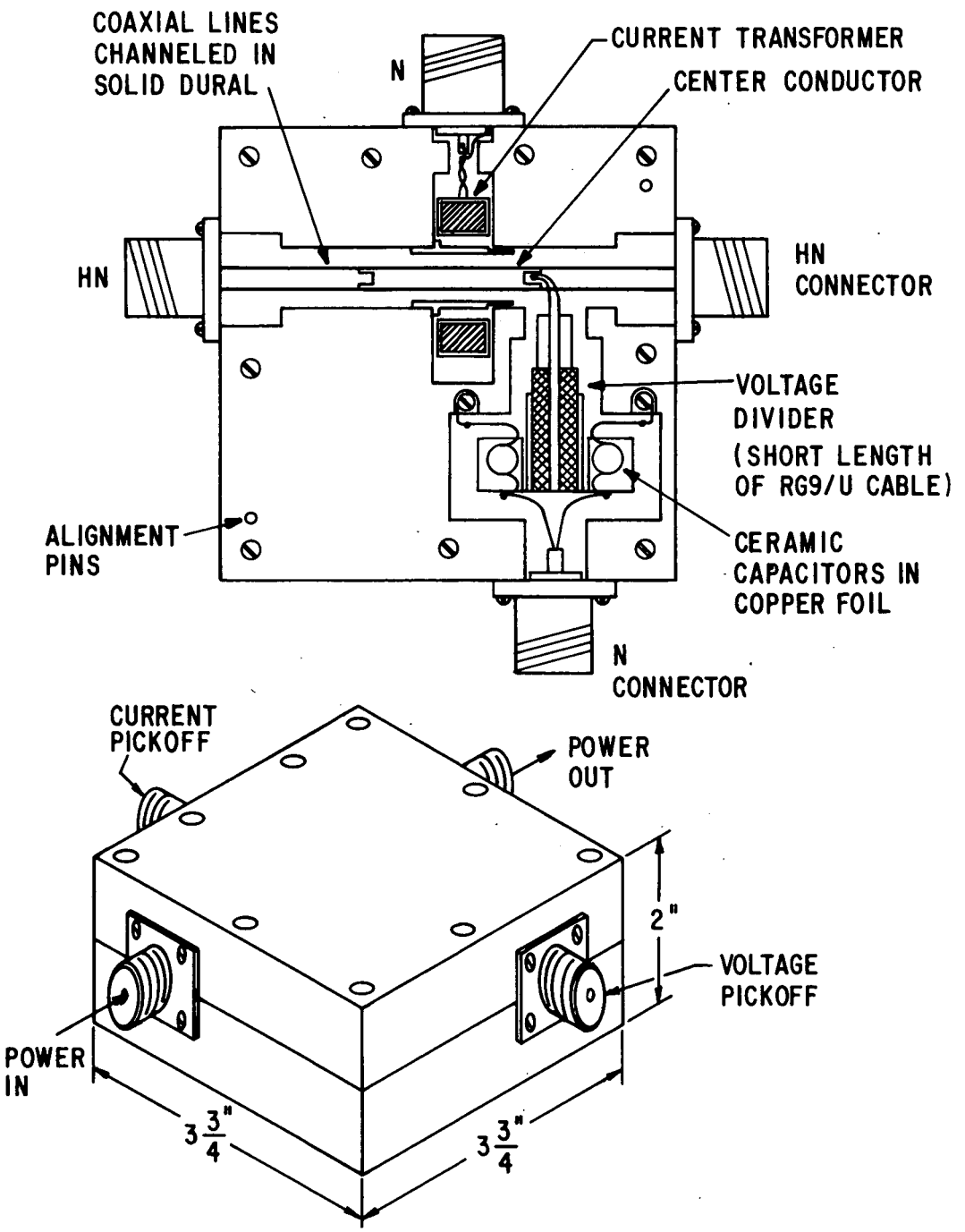

Figure 21. **Sketch of the voltage and current pickoff assembly. The shell is machined from solid Dural for stability. Current sensing is with a current transformer, and voltage sensing is with a capacitive divider. The frequency of operation in this work was 13.56 MHz, but use could be over a wide frequency range with proper design.**

The same light level was reestablished with the lamp operating at 13.56 MHz while power (in a range near 700 W) was being measured with our power measuring setup. Both procedures agreed within 2% in final calibration of our setup.

The water-cooled load was instrumented to accurately measure the difference in temperature of the entering and exiting cooling water. Also the water flow was measured with a Flow Measurement Systems, Inc. Model FMT-N5-L48 turbine-type flowmeter whose stated accuracy was + 0.2% over a 10 to 1 flow range. We found this arrangement to give a power indication 1% higher on the average than that of the Model DW wattmeter. The 60 Hz wattmeter was taken as correct. The corrected water-cooled load calibration factors were used to update the oscilloscope power calculation program described earlier in this Appendix.

Some difficulty was experienced in using the DRB lamp. At 13.56 MHz, the lead-in wires in the base of the lamp had appreciable R.F. resistance, and heated the base to such an extent that solder was melted. The base was mostly removed from the lamp and connection made directly to the feed through wires. In order to get good agreement with the other procedure, the loss in the lead-in wires had to be calculated based upon R.F. resistance measured earlier for similar wire. Furthermore, the inductive reactance of the lamp and lead-in wires had to be cancelled with a series-resonant, low-loss vacuum capacitor.

In an actual application, our power measuring setup will need to function with phase angles other than zero. To check its ability to do this, a low-loss capacitor was shunted across the 51 Ω water-cooled load to bring the angle to about 45 degrees. The instrumentation still measured the actual power loss. The result was within 1%. Also the capacitor alone was used as a load to be certain that the power indicated was zero when the angle was 90 degrees.

Appendix D

ELECTROMAGNETIC WAVE SKIN DEPTH CONSIDERATIONS

The current response, and depth of penetration into a conductor, for an applied electromagnetic field parallel to its surface, is strongly determined by the frequency of the field. At low frequencies or dc there can be a deep penetration of the field after eddy currents have been allowed time to damp. As the frequency increases, eddy currents progressively reduce the extent of penetration by countering the applied magnetic field. This should be called the magnetic skin depth by contrast to the electric skin depth associaed with surface polarization of a conductor by an electric field normal to its surface.

At still higher frequencies, above the electron plasma resonance frequency, ν_p, the electrons are inertially constrained from strong response and once again a penetration of the applied field is obtained. The applied field (wave) goes from an evanescent wave to a propagating wave, group velocity less than that in free space, above the frequency of plasma resonance. A convenient expression can tell us that the plasma frequency is

$$\nu_p = 9000\sqrt{n} \tag{D-1}$$

where n is the free electron density per cm^3. At the electron density found in HID metal halide lamps, namely $\sim 10^{15}$/cc, the electron plasma resonance frequency is 284.6 GHz. We propose to excite the plasma at a frequency of 13.56 MHz. There is thus some considerable question about depth of penetration of the exciting field.

Fortunately, for HID discharge plasmas the electron-atom collision frequency is rather high, typically $\sim 10^{11}$/s, and this again has a constraining effect on the electron response. When the ratio of electron collision frequency, ν_e, to the angular excitation frequency, $\omega = 8.52 \times 10^7$, becomes greater than one (in our case it is $\sim$1,170) penetration becomes a possibility.

There is a general expression [25] for skin depth which applies in our case,

$$\left(\frac{\lambda_o}{2\pi\, S_e}\right)^2 = 1/2 \left[\frac{(1-\frac{\omega_p^2}{\omega^2})^2 + (\frac{\nu_e}{\omega})^2}{1+(\frac{\nu_e}{\omega})^2}\right]^{1/2} - \frac{1-\frac{\omega_p^2}{\omega^2} + (\frac{\nu_e}{\omega})^2}{1+(\frac{\nu_e}{\omega})^2}, \tag{D-2}$$

where S_e is the skin depth in the same units as chosen for the free space wavelength, λ_o. The expression applies when the applied frequency is lower than the plasma resonance frequency. Now, for our case, the typical metal halide lamp plasma was dominated, in so far as electrical characteristics are concerned, by the mercury fill. If the mercury vapor is $\sim$3 atmospheres pressure when the lamp is hot, ν_e is $\sim 1.2 \times 10^{12}$s on the discharge central axis and electron density is $\sim 10^{15}$/cc. For this case, at 13.56 MHZ, S_e calculates to 2.82 cm. Observation of the SEF/HID lamp, when operating, tells us that the bright discharge channel is about 0.5 cm in diameter. Furthermore, the highest conductivity exists only in the central axis and it falls radially. Thus, it can be assumed that the applied field at 13.56 MHz completely penetrates the plasma for our case. The consequence of this is that the arc should have the same appearance as for dc or low frequency excitation, and indeed this is the case.

Given the above ν_e and N we can quickly calculate the plasma conductivity on the central axis from

$$\sigma_{dc} = \frac{n\ e^2}{m\ \nu_e} \tag{D-3}$$

where e and m are electron charge and mass. This becomes σ_{dc} = 23.44 mhos/m or a resistivity of 0.04266 Ω per cubic meter or 4.266 Ω per cubic centimeter.

It may be of interest to compare the above with the RF conductivity at 13.56 MHz. An approximate expression for conductivity under our conditions is,

$$\sigma_{rf} = \frac{n\ e^2}{m}\left[\frac{\nu}{\nu^2 + \omega^2} - j\ \frac{\omega}{\nu^2 + \omega^2}\right] \tag{D-4}$$

which calculates to

σ_{rf} = 23.44 - j 1.664 X 10^{-3} mhos/m

or

σ_{rf} = 0.2344 - j 1.664 X 10^{-5} mhos/cm

It is clear that the reactive component is small and that the resistive component, for all purposes, equals that at dc. One should not confuse this "inertial" response of the electrons, which gives the reactive component above, with the inductance of the plasma ring. The latter introduces a phase angle between the voltage applied to the plasma ring by the changing induction of the coupling transformer and the net current response of the plasma. This inductance is calculated by conventional inductance formulas as might be found, for instance, in Grover's book.[26]

It might be helpful to give some further examples. The high pressure sodium lamp, used extensively for roadway lighting, has typical parameters, n ~2 X 10^{16} electrons/cc and ν_e ~1.3 X 10^{12}/s. [27] The dc conductivity = 432.8 mhos/m or 4.328 mhos/cm while S_e = 0.655 cm at 13.56 MHz. This is for the central axis. Because the arc is narrow (wall radius might be ~0.4 cm, and region of high conductivity ~0.2 cm radius) we can again assume, for practical purposes, that the applied field very nearly penetrates the column uniformly, although the case is not as strong as for the metal halide lamp. Further calculation shows that for the high pressure sodium lamp,

σ_{rf} = 432.8 - j 0.0284 mhos/m

or

σ_{rf} = 4.328 - j 2.84 X 10^{-4} mhos/cm.

Turn finally to the case of the conventional fluorescent lamp, for instance a lamp with one inch cross sectional diameter (T-8). Filled with a rare gas, say argon at 3 torr pressure, and with mercury vapor at a reservoir temperature of 40 °C, typical parameters might be n_e = 2 X 10^{12} electrons/cc and ν_e = 1.1 X 10^9/s at the peak of the power line half cycle. For this, S_e = 1.839 cm. The diameter of a conventional F-30 lamp is 1.0 in.

(2.54 cm). Again we can say that field penetration is mostly complete when it is realized that conductivity falls radially and that the region of high conductivity might be a radius $\sim$ 1 cm. The excitation field would usually be applied longitudinally and uniformly around the lamp diameter, which helps the situation markedly. Still, if accurate calculations are to be made, skin depth may be important in the fluorescent lamp, especially for the more highly loaded lamps. For the above parameters,

σ_{dc} = 51.15 mhos/m or 0.512 mhos/cm

σ_{rf} = 50.84 - j 3.94 mhos/m

σ_{rf} = 0.5084 - j 0.0394 mhos/cm

Note that the reactive component is somewhat larger than for earlier HID lamp examples.

Appendix E

IMPEDANCE MATCHING CONSIDERATIONS

We are faced with the problem of electrically matching the discharge plasma of the lamp to the power source. Commercially available power sources generally supply power to a load through a coaxial cable whose characteristic impedance is purely resistive at 50 Ω. The lamp plasma in our case is a conducting ring which has both resistance and reactance. The reactance of the plasma is not due to any inertial response of the free electrons, as might be the case if the electron-heavy particle collision frequency was quite low and the electrons could receive and return energy to the electric field without loss by momentum exchange. But rather it is due to the straightforward establishment of a magnetic field by the current flow in the plasma, and energy storage and return between the field and the current as would be the case in a common wire loop.

We have chosen to excite the plasma by the electric field from a changing magnetic field. The magnetic field is produced by a solenoid of wire. The resulting solenoid and plasma ring are thus describable as a transformer with the solenoid as the primary and the plasma as secondary. The input impedance looking into the primary is quickly found by circuit theory and is described by Equation A-1 of Appendix A. For our case the input impedance can be regarded as an impedance composed of a series combination of resistance and inductive reactance. This includes the reflected resistance and reactance discussed in Appendix A. Stray capacitance across the primary solenoid and in the wiring has the effect of increasing the impedance looking into the primary as described by Equations B-3 and B-4 of Appendix B.

The problem is resolved at this point to matching the pure resistance of the power supply cable to an impedance which is a series combination of resistance and reactance, i.e. that which would be seen if one looked at Z_4 of Figure 5. This can be accomplished by a series combination of capacitors as is well known, see Reference 21, page 148. We can refer to Figure 22 for the appropriate circuit. The matching capacitors are C_1 and C_2. The value of C_2 can be chosen so that the series combination of its reactance and the reactance of X_p give a net inductive reactance, referred to as X_{p2} on Figure 22b. Now the incoming line at point A looks into a parallel combination of X_{p2} and C_1, which can be resonated at 13.56 MHz by the proper choice of C_1 to offer a pure resistance between points A and G. The transformed value of R_p can match the 50 Ω cable by an overall choice of the ratio of C_1 and C_2. The algebra to prove the above is straightforward, but tedious.

In our case the impedance matching is accomplished by capacitors located in an aluminum box near the lamp in the integrating sphere. A length of RG 9/U cable, 84 cm long, connects this box with the point outside the sphere where cable voltage and current are sensed. If the matching network is carefully adjusted so that 50 Ω is presented to the line inside the sphere, the sensors see a "flat" line and detect 50 Ω when looking into the short length of RG 9/U cable. It is not important to our work that an exactly 50 Ω match is effected in the sphere. If there is a mismatch, there are standing waves on the line and the impedance that the sensors see may be other than 50 Ω and in fact complex. It is necessary for the overall calculation of power to the lamp that the impedance transformation caused by the length of RG 9/U cable be known. If Z_r is the receiving end impedance (in the sphere) and Z_s is the sending end impedance (at the sensors) the transformation is found in any textbook which treats transmission line theory, for instance Johnk (Reference 29),

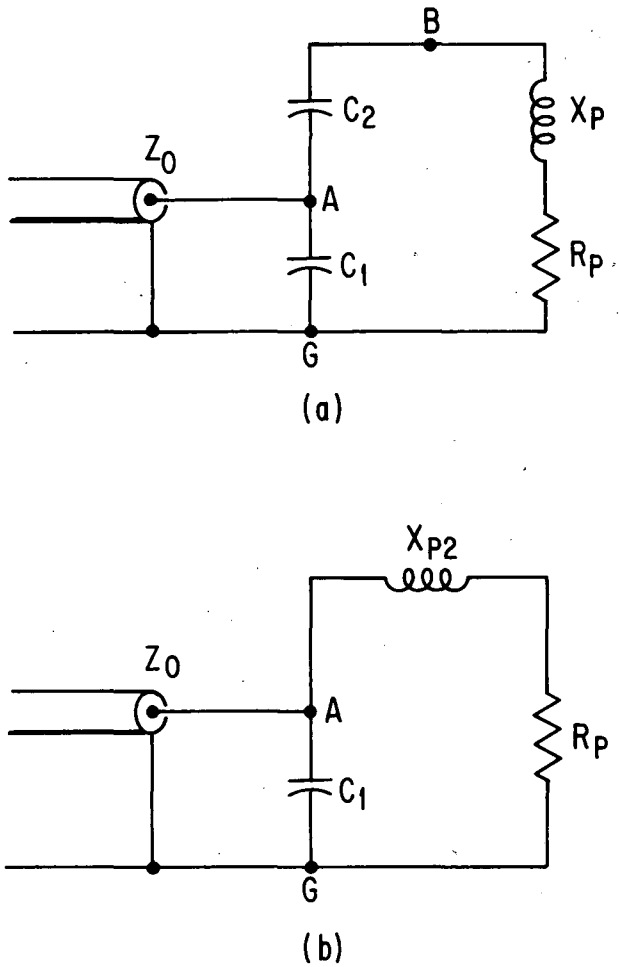

Figure 22. Simplified sketches of the matching network between the coaxial transmission line and the primary coil which couples to the lamp plasma secondary.

$$Z_s = Z_o \left[\frac{Z_r \cos \beta l + j\, Z_o \sin \beta l}{Z_o \cos \beta l + j\, Z_r \sin \beta l} \right] \tag{E-1}$$

In our calculation we start with the measured values of voltage and current and the phase between them at the sensors and calculate Z_s in (E-1). To calculate Z_r a small amount of algebra puts (E-1) into the form of Equation (2), which is more useful. In the evaluation of Equation (2) the β used must be that in the cable, which is different than for free space. In free space a wave in the TEM mode has a velocity of propagation of 30 cm/ns. In the cable the velocity is 20.92 cm/ ns. Thus $\beta = 2\pi/\lambda$ in the cable is 0.4074 rad/m. Our length of cable is 0.8382 m and Equation 2 reduces to

$$Z_r = \left[\frac{(47.115)(Z_s) - j\,837}{47.115 - j\, Z_s\,(0.3348)} \right] \tag{E-2}$$

With the use of Equation (E-2) the impedance 111.77 + j 18.78 Ω given in the sample calculation of Section "Experimental Procedure and Sample Calculation" transforms to 65.71 + j 46.94 Ω, also noted in that Section.

It is also important to the experiment that the geometry chosen to terminate the cable in the sphere be such that no large currents at 13.56 MHz flow on the outside of the enclosure for the matching capacitors. This could lead to additional loss. Thus, the capacitors are wired within the aluminum box so that heavy currents are confined to copper braid conductors of low inductance and resistance, and the braid is terminated at points where the current is expected to go. On Figure 23 we can see a simplified drawing of the circuit. The sensors are located at points A/B and read voltage and current on the line. Line current flows into the matching capacitors C_1 and $C_2$and returns directly in all cases to inside surface of the outer conductor of the coaxial cable. The magnetic field from the coil induces some currents to flow on the outside of the enclosure but these lead to little loss because of the silver sheet under the coil. The silver also reflects light from the discharge plasma with very little loss. Thus it is seen that power on the line and into the matching network and primary coil can be measured at points A and B under reasonably well matched conditions. Even if matching is not perfect the time averaged values of v and i at the sensors will give power delivered to the lamp assembly.

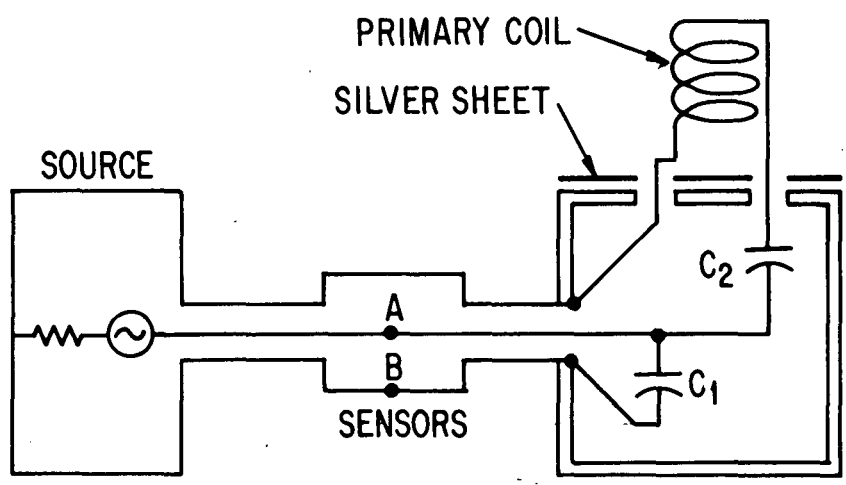

Figure 23. Schematic of the relation between the primary coil and the power source, showing that large power-carrying currents are constrained to flow on the cable interior and in the shielding enclosure except for a brief excursion through the primary coil.

This report was done with support from the Department of Energy. Any conclusions or opinions expressed in this report represent solely those of the author(s) and not necessarily those of The Regents of the University of California, the Lawrence Berkeley Laboratory or the Department of Energy.

Reference to a company or product name does not imply approval or recommendation of the product by the University of California or the U.S. Department of Energy to the exclusion of others that may be suitable.

TECHNICAL INFORMATION DEPARTMENT
LAWRENCE BERKELEY LABORATORY
UNIVERSITY OF CALIFORNIA
BERKELEY, CALIFORNIA 94720